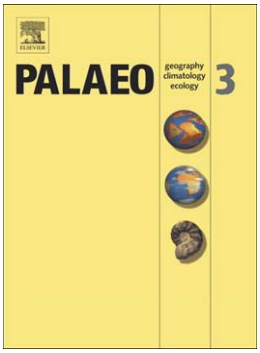

Biological and physical evidence for extreme seasonality in central Permian Pangea

Cindy V. Looy, Stephanie L. Ranks, Dan S. Chaney, Sophie Sanchez, Sébastien Steyer, Roger M.H. Smith, Christian A. Sidor, Timothy S. Myers, Oumarou Ide, Neil J. Tabor

PII: S0031-0182(16)00090-0
DOI: doi: 10.1016/j.palaeo.2016.02.016
Reference: PALAEO 7691

To appear in: *Palaeogeography, Palaeoclimatology, Palaeoecology*

Received date: 25 February 2015
Revised date: 1 February 2016
Accepted date: 9 February 2016

Please cite this article as: Looy, Cindy V., Ranks, Stephanie L., Chaney, Dan S., Sanchez, Sophie, Steyer, Sébastien, Smith, Roger M.H., Sidor, Christian A., Myers, Timothy S., Ide, Oumarou, Tabor, Neil J., Biological and physical evidence for extreme seasonality in central Permian Pangea, *Palaeogeography, Palaeoclimatology, Palaeoecology* (2016), doi: 10.1016/j.palaeo.2016.02.016

Biological and physical evidence for extreme seasonality in central Permian Pangea

Cindy V. Looy[a], Stephanie L. Ranks[a], Dan S. Chaney[b], Sophie Sanchez[c], Sébastien Steyer[d], Roger M. H. Smith[ef], Christian A. Sidor[g], Timothy S. Myers[h], Oumarou Ide[i], Neil J. Tabor[h]

[a]*Department of Integrative Biology and Museum of Paleontology, University of California, Berkeley, Berkeley CA 94720, USA*

[b]*Department of Paleobiology, NMNH Smithsonian Institution, Washington, D.C. 20560, USA*

[c]*Department of Physiology and Developmental Biology, Evolutionary Biology Centre, Uppsala University, Norbyvägen 18A, 75236 Uppsala, Sweden*

[d]*Centre de Recherches en Paléobiodiversité et Paléoenvironnements (UMR 7207 CNRS-MNHN-UPMC), Muséum national d'Histoire naturelle, CP 38, 8 rue Buffon, F-75008 Paris, France*

[e]*Karoo Palaeontology, Iziko: South African Museum, Cape Town 8000, South Africa*

[f]*Evolutionary Studies Institute, University of Witwatersrand, 1 Jan Smuts Avenue, Johannesburg 2000, South Africa*

[g]*Burke Museum and Department of Biology, University of Washington, Seattle, Washington 98195, USA*

[h]*Huffington Department of Earth Sciences, Southern Methodist University, Dallas TX 75275-0395*

[i]*Institut de Recherches en Sciences Humaines, Niamey, Niger Republic*

Corresponding author: Cindy V. Looy

Address: 1005 Valley Life Sciences Bldg #3140, Berkeley CA 94720-3140

Phone: ++1-510-642-1607

E-mail: looy@berkeley.edu

Abstract

Climate models indicate increased desertification in the continental interior of Pangea during the Permian, which would have affected the composition of the flora and fauna. We present a multi-proxy paleoenvironmental reconstruction of a terrestrial ecosystem in central Pangea of Lopingian age. The reconstruction is based on biological and physical data from the Moradi Formation, located in the Tim Mersoi Basin, northern Niger. Paleosols and sedimentological evidence indicate that the prevailing climate was semi-arid to very arid with marked intervals of high water availability. Carbon stable isotope data from organic matter and paleosols suggest that both the soil productivity and actual evapotranspiration were very low, corresponding to arid conditions. Histological analysis of pareiasaur bones shows evidence of active metabolism and reveals distinct growth marks. These interruptions of bone formation are indicative of growth rhythms, and are considered as markers for contrasting seasonality or episodic climate events. The macrofossil floras have low diversity and represent gymnosperm-dominated woodlands. Most notable are ovuliferous dwarf shoots of voltzian conifers, and a 25-m long tree trunk with irregularly positioned branch scars. The combined biological and physical evidence suggests that the Moradi Formation was deposited under a generally arid climate with recurring periods of water abundance, allowing for a well-established ground water-dependent ecosystem. With respect to its environment, this system is comparable with modern ecosystems such as the southern African Namib Desert and the Lake Eyre Basin in Australia, which are discussed as modern analogues.

Keywords

Niger, Permian, Central Pangea, climate, desert, paleobiology

1. Introduction

Lithological and phytogeographic data show that the region currently forming the interior of Africa experienced increased aridification from the Late Carboniferous-early Permian to the middle to late Permian (Gibbs et al., 2002; Rees et al., 2002). Climate models estimate that desert-like conditions prevailed in central Pangea during the Lopingian, with most recent models suggesting summertime high temperatures around 40-50° C (Fluteau et al., 2001; Peyser and Poulsen, 2008; Kiehl and Shields, 2005). The change from seasonally wet Cisuralian climate to desert-like Lopingian climate must have considerably altered both the composition of the flora and fauna in the local communities, and also their potential pathways for dispersal (Sidor et al., 2005). How exactly the biota responded is difficult to assess, however, as arid climates typically do not create the best conditions for plant preservation (Gastaldo and Demko, 2010), leaving an unsatisfactory gap in our knowledge of central Pangean ecosystems.

Fortunately, rare fossil vertebrate and plant assemblages have, in the past ten years, been discovered from the Upper Permian in northern Niger (Damiani et al., 2006; Sidor et al., 2003, 2005; Smiley et al., 2008; Steyer et al., 2006; Tsuji et al., 2013; Turner et al., 2015). During Lopingian times, deposition of the Moradi Formation of the Tim Mersoi sub-basin, Iullemeden Basin, occurred approximately 10° S of the paleoequator in central Pangea. Studies of vertebrate fossils from the Moradi Formation have suggested a community structure and taxonomic composition similar to those described from Morocco (e.g. Germain, 2010; Jalil and Dutuit, 1996; Jalil and Janvier, 2005; Sidor, 2013; Steyer and Jalil, 2009). They are, however, distinctly different from any of the better understood southern Pangean assemblages (e.g. South Africa, Tanzania, Zambia, and Malawi), which were dominated by therapsids (e.g. Angielczyk et al., 2013; Sidor et al., 2005, 2013). The faunas from Niger and Morroco both are dominated by temnospondyls, pareiasaurs, and captorhinids. The two herbivorous reptiles described from the Moradi Formation of Niger, the captorhinid *Moradisaurus* and the pareiasaur *Bunostegos*, are known only from

the formation (de Ricqlès and Taquet, 1982; Sidor et al., 2003; Taquet, 1969; Tsuji et al., 2013; Turner et al., 2015). Similarly, both of the temnospondyls described, *Nigerpeton* and *Saharastega*, represent relicts, or holdovers of lineages represented in faunas thought to have gone extinct near the Pennsylvanian-Permian boundary elsewhere (Damiani et al., 2006; Sidor et al., 2005, 2013; Steyer et al., 2006). The only terrestrial predator discovered in these faunas is represented by fragmentary gorgonopsid remains, not sufficient for a generic identification (Smiley et al., 2008). Due to the lack of any obvious physical barrier between the faunas of central and southern Pangea Sidor et al. (2005) hypothesized that climate was the factor likely responsible for the biogeographic isolation and endemism of the Moradi assemblage.

These climatic interpretations are corroborated by sedimentary, morphological, and mineralogical data from paleosol profiles in the Moradi Formation, which display evidence of prevailing arid conditions at the time of development. (Tabor et al., 2011; Smith et al., 2015). The paleosols and associated sedimentary strata are characteristic of those formed under a range of conditions from well to poorly drained, and represent stable floodplains of ephemeral, anabranching fluvial depositional systems (Tabor et al., 2011). These soil types are indicative of semi-arid areas with relatively shallow water tables, and include those formed on plains surrounding ephemeral lakes or playa environments. Modern analogues of these soil types can be found in the Namib Desert (Watson, 1992) of southwestern Africa and the Lake Eyre Basin, central and eastern Australia (Tabor et al., 2011; Fielding and Alexander, 2001; Tooth and Nanson, 2000). Both fossil and extant landscapes represent Heinrich Walter's zonobiome 3, or hot and arid subtropical deserts with very little rain (Breckle, 2002).

In this paper new biological and physical evidence for extreme seasonality in the Moradi Formation are presented, using a wide array of ecological proxies. The paleosol and sedimentological data are described briefly, and the stable carbon isotope compositions of paleosol calcite and co-existing organic matter are presented and discussed in terms of their relevance to interpretations of paleoclimate, biological productivity and water availability for floral and faunal communities across these paleolandscapes. Data

from tetrapod bone histology is presented for evidence of seasonality, including cyclical periodic cessation of growth. The Moradi gymnosperm-dominated fossil floras, including a large tree trunk, are described for the first time, and compared to modern analogs in order to constrain the environmental circumstances under which these plants grew. Finally, the implications of the combined data on the interpretation of climate for Lopingian central Pangea are discussed.

2. Material and methods

2.1. Geological setting

The Carboniferous-Permian stratigraphy and structural evolution of the Tim Mersoi sub-basin of the Iullemeden basin in north-central Niger was recently reviewed in Tabor et al. (2011). At the time of active Permian deposition, the basin was moving northward from ~30 to ~10° S (Scotese et al., 1999), and remained at least 2000 km from the nearest open ocean. The Moradi Formation is the terminal lithostratigraphic unit of the Izegouandane Group and, in the study area, comprises ~100 m of dominantly red mudstones with secondary fluvial channel sandstones and conglomerates as well as rare coarse breccias (Fig. 1). A Lopingian age of deposition for Izegouandane Group strata is primarily based upon biostratigraphic correlations of fossil vertebrates in the Moradi Formation to contemporaneous strata in Russia and South Africa (Sidor et al., 2005; Lucas, 2004; Taquet, 1969).

The specimens described in this paper were collected from several localities located approximately 20 km west of Arlit, Agadez Department, northern Niger (see o'Keefe et al., 2005 or Damiani et al., 2006 for a map of the study area). The localities are within 1 km of each other and all fall within the upper half of the Moradi Formation. Detailed locality data are available to qualified researchers at the Musée National du Niger in Niamey (MNN) or by contacting Christian A. Sidor. The fossil material described here is housed in the paleontological collections at the MNN.

2.2. Sedimentary environment and taphonomy of plant fossil localities

The upper Moradi succession is made up of three distinctive associations of sedimentary facies, which were interpreted as having accumulated in discrete sub-environments of the Moradi alluvial plain. These are (1) high sinuosity channel fill and point bar, (2) loessic floodplain and incised distributary channels, and (3) end-point playa. The stratigraphic position and sedimentological log of the fossil localities recovered by our team in the 2003 (S) and 2006 (T) expeditions is shown in Figure 1. The plant fossils from locality T9 occur within the loessic floodplain facies in a 0.25m-thick bed of pale red massively-bedded calcareous siltstone ("siltite") with olive mottling along vertically orientated, downward branching root molds. This facies directly overlies a 3 m-thick conglomeratic sandstone displaying gently dipping (+/-20^{o}) beds on its upper surface, which are interpreted as lateral accretion units of a large low-angle point bar. The fossiliferous "siltite" is immediately succeeded by a sequence of carbonate mudrock breccia and thinly-bedded micritic limestone interpreted as the accumulated deposits of a semi-permanent playa lake that most likely formed at the end-point of an ephemeral distributary channel (Smith et al., 2009, 2015). For a paleogeographic map and more information on the study area see Smith et al., 2015.

The leaf fossils occur as three-dimensional molds scattered at random orientations throughout the pale red siltstone, rather than concentrated along horizontal bedding planes. The lack of clearly-defined bedding planes within a bed of homogeneous unsorted silt-sized grains suggests that the leaf-bearing bed was deposited in a single episode and fairly rapidly as is common in windstorm-generated loess (Giles et al., 2013). The presence of root channels and the pervasive carbonate cement are indicative of incipient pedogenesis with relatively high water-tables in an evaporative setting, such as would be encountered on the sparsely-vegetated margins of an arid zone floodplain lake.

2.3. Fossil Flora

Fossil plants were observed and collected from a total of three localities (Fig. 1). Two (field localities T09 and T24) produced vegetative remains and one (field locality T25) produced fossil wood. Localities T09 and T24, in the upper part of the Moradi Formation, produced vegetative and fertile plant fossils in the

form of dark rust-colored carbonaceous dust in three-dimensional molds of a lighter colored fine-grained siltstone. The material was photographed using a Nikon D300 with a 60mm macro lens. Leaf fossils were found at both localities. Ovuliferous dwarf shoots of a voltzian conifer were found only at T24. Of the sixty-one dwarf shoots collected, twenty-eight were selected for morphological measurements based on well-defined outlines and completeness. Because terminology used to describe ovuliferous cones of early conifers deviates from that for modern species, terms used herein are explained (see Hernandez-Castillo et al. 2001; Rothwell et al. 2005). ‘‘Bracts’’ are foliar appendages of the cone (or fertile zone) axis, these are interpreted as a modified leaves. ‘‘Ovuliferous dwarf shoots’’ or “dwarf shoots” are lateral branches of limited growth, arising in axils of the bracts. A “sporophyll” is a potentially seed bearing appendage of an ovuliferous dwarf shoot, while a ‘‘sterile scale’’ is a foliar appendage.

Locality fossil forest deposit (field locality T25). One fossil tree trunk was partially excavated to a length of 25 m. The log was oriented roughly around 0° N-S with a dip of ~02° degrees. The angle of the fossil tree trunk arises from deposition at an orthogonal angle upon a point-bar deposit of a meandering stream. The length, diameter, branch base positions and shape of the exposed surface of the prone trunk were recorded. Small greenish-gray (silicified) wood samples were collected from the lower part of the trunk. These samples were thin-sectioned using standard techniques employed for petrified plant fossil material (e.g., Hass and Rowe, 1999). In the immediate area (< 0.1 km^2) around the excavated log, there were other green haloes in the red sediment, as well as mounds of fragmented petrified wood. Petrified wood fragments also were found near vertebrate-producing sites S44 and S48, upon microscopic examination, no cellular structures were observed.

2.4. Paleosols and carbonate samples for geochemical analysis

The geochemical part of this study focuses on $\delta^{13}C$ values of paleosol calcite and co-existing organic matter samples from 23 different paleosol profiles distributed among three different stratigraphic sections

of the Moradi Formation. The paleosols from which these samples were collected exhibit three distinct morphologies (Tabor et al., 2011).

Paleosol type A: Type A paleosols occur in very fine to medium sandstones, and are especially common within the upper 1–2 m of thick sandstones that preserve trough cross-strata. They include vertical to horizontal calcareous tubules ranging from 1-100 mm in diameter, and ~10 mm to 3.7 m in length that are interpreted to be rhizoliths (*sensu* Klappa, 1980) or root petrifactions (Tabor et al., 2011). Rhizoliths are typically composed of micritic calcite with alveolar texture on the exterior of the tubule and void-filling sparry calcite crystals on the interior of the tubule that grew inward. They rarely occur in such abundance that they dominate the volume of stratigraphic horizons, and are similar to calcified root mat horizons that have been interpreted to form just below the groundwater table (Wright, 1990). This paleosol type also rarely includes stratiform calcareous layers near the base of profiles that are interpreted to be groundwater calcrete (*sensu* Semeniuk, 1985, 1981; Fig 3F).

Paleosol type B: Type B paleosols occur in blocky red mudstones and include an abundance of discrete carbonate nodules, vertically stacked carbonate nodules (*sensu* Blodgett, 1988) and vertically and horizontally orientated carbonate tubules composed of micritic calcite. Calcareous nodules are interpreted to be stage II pedogenic nodules (*sensu* Machette, 1985), whereas calcareous tubules are interpreted as rhizoliths (Klappa, 1980). These paleosol profiles are typically noncalcareous in the upper ~15 cm of the profiles. Below that level they often include micritic calcareous cements along the exteriors of mudstone blocks; these are interpreted to be pedogenic calcans (Tabor et al., 2011).

Paleosol type C: Type C paleosol profiles occur in red mudstones that exhibit wedge-shape aggregate structure and low-angle slickenplanes. Profiles of this paleosol type are noncalcareous in the upper 15-30 cm of the profiles, but carbonate nodules and concretions ranging from a few mm to about 50 mm in

diameter and irregular carbonate tubules are common (5-20% by volume) to abundant (>20% by volume; Tabor et al., 2011).

In addition to the carbonate in the paleosol profiles discussed above, early-burial groundwater calcite and void-filling sparry calcite cements also are found in association with these paleosol profiles. Several examples of each are included in this work for comparison of stable carbon isotope compositions with micritic calcite nodules, tubules and calcans in paleosol profiles.

2.5. Stable carbon isotope geochemistry

Carbonate samples that were collected from at least 50 cm beneath the interpreted paleo-surface of paleosol profiles were drilled directly from thin-sections, matching billets, or polished slabs using a table-top drill system with 100 mm diamond bits on an x, y, z stage. Between 2 and 20 mg of carbonate-bearing powders were loaded into reaction vessels, and atmospheric gases were evacuated. Samples were then dissolved in 100% H_3PO_4 *in vacuo* at 25° C for about 16 hours to produce CO_2. CO_2 samples were cryogenically purified, and CO_2 yields were determined via mercury manometer with a precision of ±0.2 µmol. The resulting CO_2 was analyzed for carbon and oxygen isotope ratios using a Finigan MAT 252 isotope ratio mass spectrometer at Southern Methodist University.

Although fossil macroplant impressions and petrifactions occur in the Moradi Formation (reported in this paper), macroscopic examples of fossilized organic plant matter were not observed. However, several examples of paleosol carbonate nodules and tubules occlude finely disseminated, organic-rich domains. These paleosol carbonate samples were pulverized, acidified in concentrated (~12 N) HCl in order to dissolve carbonate and eliminate it as a possible undesirable source of carbon during pyrolysis of organic matter. The organic-enriched residue was then rinsed with ionized water until the rinse water remained at the original pH (~5.6) after at least 10 minutes of contact with the acid-leached sample. The residues were then freeze-dried to remove absorbed water. The carbon content and $\delta^{13}C$ values of the samples were

determined from CO_2 produced by closed system combustion of the organic matter following the methods of Boutton (1991).

In order to provide a context for the interpretation of Moradi Formation paleosol calcite and organic matter $\delta^{13}C$ values, paleosol carbonate and organic matter from three other Middle and Upper Permian basins are included in this work. These include the Middle and Upper Permian Quanzijie and Wutongguo formations of the Turpan Basin, Xinjiang Province, northwestern China (Yang et al., 2010). Samples from the Quanizijie Formation were collected from two different paleosol profiles in the lower half of the Formation (see Yang et al., 2010 for the specific lithostratigraphic section). Also included are calcite and co-existing organic matter stable carbon isotope compositions from Upper Permian (Changhsingian) Balfour Formation, South Africa (Gastaldo et al., 2013; Gastaldo et al., 2014), and Upper Permian Buntsandstein Formation, Italy.

Isotope values are reported in standard delta notation:

$$\delta^{13}C = (R_{sample}/R_{standard} -1)*1000,$$

where R is the ratio of heavy to light stable isotope present in the sample or standard, and δ values are reported relative to the Peedee Belemnite standard (PDB; Craig 1957) for both carbon and oxygen isotope ratios.

2.6. Bone histology

Four isolated pareiasaur bones, provisionally referred to *Bunostegos akokanensis* (humerus – MNN MOR145, radius – MNN MOR146, ulna – MNN MOR147, scapula – MNN MOR148), were sampled from the Moradi Formation at locality T22 (Tabor et al., 2011). The fossil material is preserved in three dimensions. The bones were prepared for osteohistology and embedded in resin (Lamm, 2013). The long

bones were sectioned at mid-shaft and a thin section was made just dorsally to the narrowest region of the scapula. They were observed and photographed using optical microscopes (Nikon Eclipse 80i and Leica CTR6000) with either ordinary transmitted light or polarized light.

The skeletochronological analysis (Castanet et al., 1993) that was performed consists of blind counting the number of growth marks that remain visible in the appositional deposit of compact primary tissue. A growth mark is composed of (1) a zone, corresponding to the amount of bone rapidly deposited during favorable periods of food supply; (2) an annulus, made of lamellar bone formed when environmental conditions become poorer; and in extreme cases, (3) a line of arrested growth (LAG) when the animal needs to reduce their metabolism and enter into lethargy or dormancy for survival (e.g., hibernation, aestivation; Castanet et al., 1993). LAGs are thus considered as biomarkers of contrasted seasonality. Growth marks are evidence of biological cycles interspersed throughout tetrapod bones. They have been intensively studied among extant species with regard to their age and development (Castanet, 1994; Castanet and Baez, 1991; Castanet et al., 2003). Growth mechanisms of periosteal bone are similar for all tetrapods, and thus can be assumed to be so for fossils (de Ricqlès, 1981, 1975; de Ricqlès et al., 2004). Therefore, growth marks are a proxy for the reconstruction of fossil tetrapod life history traits (e.g. Köhler et al., 2012; Sanchez et al., 2008, 2010b; Scheyer and Sander, 2009; Steyer et al., 2004) and the palaeoecological conditions influencing them (e.g. Konietzko-Meier and Klein, 2013; Sanchez and Schoch, 2013; Sanchez et al., 2010a; Steyer et al., 2004).

3. Results

3.1. Fossil flora

Systematics:

Leaves – The macrofloral elements from the two plant localities produced four morphological leaf types.

Description:

Morphotype 1: (T09, T24; 28 specimens) Isolated narrow strap-like leaves. These leaves were the only type found at the T24 locality. They are linear, straight to slightly curved, ranging between 100-125 mm in length and 2.2-3.5 mm in width (Fig. 2A). They taper slightly at their square base and have obtuse apices.

Morphotype 2: (T09; 2 specimens) Isolated linear leaves of variable size, approximately 85-133 mm long by 5-11 mm wide, with obtuse apices (Fig. 2B). The base is unknown. The leaves have prominent striations running parallel to the leaf margin (see inset). These striations could represent veins or stomatal rows.

Morphotype 3: (T09; 2 specimens) Shoot fragments with leaves. The leaves are short and narrow, linear, 5-22 mm long and 0.5-1.2 mm wide, with obtuse apices (Fig. 2C-D). They arise from the axis at angles between 26 -75 degrees.

Morphotype 4: (T09; 4 specimens) Shoot fragments with obovate leaves. Leaves are 9-21 mm long and 2.2-3.6 mm wide, with obtuse tips and have slightly to greatly tapered bases that attach at angles of 12-50 degrees (Fig. 2 E-F).

Ovuliferous dwarf shoots – (T24; 61 specimens) The dwarf shoots have at least ten partially fused scales that are flattened and bilaterally symmetrical, longer than they are wide (Fig. 3). The total length of the dwarf shoots varies from 8-21 mm and width from 9-17 mm. Each dwarf shoot bears two types of foliar elements, interpreted as sterile scales and sporophylls. The sterile scales are narrow-triangular in shape with acuminate apices and are positioned in at least two planes. They have fused bases but separate in their upper 2-7 mm, with widths of 0.2-0.7 mm immediately distal to the point of separation of the scales. The sporophylls seem to be interspersed among the sterile ones. The more centrally positioned sporophylls are oblong to triangular with a rounded apex, shorter and fleshier than the sterile scales, and

about 3.9-6.6 mm long and about 0.7-1.8 mm wide. The position of the ovule attachment area could not be discerned. The scale-bearing, fused part of the ovuliferous dwarf shoot is much wider than high *en face* with a broad, rounded base (Fig. 3C-E). The basal part is long and stalk-like, with a length ranging from 8.5-12 mm and diameter/width between 0.5-3.3 mm. It is not clear if the stalk-like base was attached to the bract. It was possible to determine the original shape of the ovuliferous dwarf shoots by the impressions left on the matrix. In one specimen, in which both part and counterpart are preserved, the fused scale-bearing part of the dwarf shoot displays a thickness of 4 mm (Fig. 3F).

Log – (T25) The exposed straight basipetal part of the Moradi tree measured 58 cm in diameter (Fig. 4). During excavation, more than 24.9 m of the trunk was exposed. As the base of the trunk is not preserved, all length measurements are from the basipetal end of the log as preserved. The basipetal end is not flared. Flaring of the trunk would suggest that the tree base was within < 0.5 m. Thus, the true base of tree, were it to have been preserved, was more than a meter below the preserved base. The distal-most exposed end of the trunk had a width of 20 cm, and continued into unexcavated strata. Based on the size of the branches that had broken off the trunk, the distal end of the preserved tree is probably not more than 1 m beyond the end of the excavation. Therefore, whether the true based was preserved or not, the length of the trunk in life was greater than the fossilized specimen, as exposed in excavation. Scars of irregularly spaced branches are present along most of the length, but are less common and not as prominent in the basal 9 m. Above 9 m the branch scars gradually increase in size. Between 9 and 11 m the elliptical branch scars range from 4 x 3 cm to 10 x 8 cm (l x w). Above 11 m, larger branch scars occur, ranging from 10 x 19 cm to 22 x 15 cm, with smaller branch scars increasingly interspersed above 19 m. At the very top of the exposed portion there is a branch scar as large as the width of the tapered trunk (10 x 10 cm), indicating that it had bifurcated at that point.

Thin sections revealed poor anatomical preservation (Poole 2013, pers. comm.), making identification of the wood problematic. No evidence for growth rings or growth intervals were observed, this however is

not to say definitively that this specimen did not have these features *in vivo*. Isolated wood fragments from other vertebrate-rich localities were identified as *Agathoxylon* (Bamford personal communication), a wood morphology characteristic of coniferophytes, cordaitaleans, and conifers (Philippe and Bamford, 2008). The cross section of the basal part of the trunk is massive and shows no evidence of a large central pith. The absence of a central pith excludes the cordaitaleans and suggests that the fossil trunk is likely a conifer. The observed irregular branching pattern is characteristic of orthotropically branching voltzian conifers (Rothwell et al., 2005).

3.2. Stable carbon isotope geochemistry

Paleosol Calcite - Paleosol carbonate samples from the Moradi Formation (n = 69) range from 19 - 100% calcite (Table 1). Among the samples analyzed, calcans and stage II carbonate nodules have lower, whereas stage III carbonate layers and rhizoliths have higher wt. % calcite (Table 2). Micrite $\delta^{13}C$ values (n = 66) range from -8.2 to 3.3‰ (mean = -3.0±1.6‰). Spar and microspar cement $\delta^{13}C$ values (n = 3) range from -4.6 to -3.4‰ (mean = -4.2±0.7).

In general, micrite from BkIII horizons and rhizoliths record the most positive $\delta^{13}C$ values, whereas BKII nodules record the most negative $\delta^{13}C$ and values. Calcans and early-burial groundwater cements record intermediate $\delta^{13}C$ values. This pattern of isotope distribution among the carbonate textures is also mimicked by the pattern of isotope distribution among paleosol carbonates with respect to their host lithology. That is, calcite from sandstone profiles generally records more positive $\delta^{13}C$ values, calcite from mudstone profiles records more negative $\delta^{13}C$ values, and calcite from siltstones has intermediate $\delta^{13}C$ values.

As mentioned, other Middle and Upper Permian paleosol carbonate samples were analyzed in order to place the Moradi Formation calcite isotope values in a broader context. Quanzijie Formation micrite samples (Middle Permian, NW China; n = 4) record $\delta^{13}C$ values between -5.2 and -3.9‰ (mean = -

4.6‰). Wutonggou Formation micrite samples (Upper Permian, NW China; n = 2) record $\delta^{13}C$ values between -13.5 and -10.4. Balfour Formation micrite samples (Upper Permian, South Africa; n = 10) record $\delta^{13}C$ values between -17.1 and -5.3‰ (mean = -11.6‰). Buntsandstein micrites (Upper Permian, northern Italy; n = 9) record $\delta^{13}C$ values between -3.2 and -5.9‰ (mean = -4.6‰). Thus, micrite $\delta^{13}C$ values from the Moradi Formation paleosol carbonates are more positive than Middle and Upper Permian samples from other sites.

Organic Matter - Residues (n = 9) from acid-reaction of carbonate nodules, rhizoliths, and calcans in the Moradi Fm. range from 0.053 – 1.187 wt. % carbon (Table 2). $\delta^{13}C$ values of CO_2 produced via pyrolysis of organic matter in these residues range from -20.8 to -24.5‰. The difference between corresponding calcite and organic matter carbon isotope values, or $\Delta^{13}C_{CC\text{-}OM}$, ranges from 18.2 to 24.4‰.

Middle Permian Quanzijie Formation residues (n = 2) have organic matter $\delta^{13}C$ values that range from -19.8 to -20.3‰, whereas $\Delta^{13}C_{CC\text{-}OM}$ values range from 15.2 to 15.6‰. Upper Permian Balfour Formation residues (n = 5) range from -25.3 to -26.6‰, whereas $\Delta^{13}C_{CC\text{-}OM}$ values range from 3.3 to 20.4‰. Upper Permian Buntsandstein and Wutonggou formations carbonate samples were not available for production of organic matter-rich residues. However, coalified branch axes and fossil leaves in close stratigraphic association with paleosol calcite samples are available for determination of organic matter $\delta^{13}C$ values. Fossil wood samples from the Bundsandstein Formation range from -21.6 to -22.6‰, resulting in $\Delta^{13}C_{CC\text{-}OM}$ values from 16.3 to 18.7‰. Organic matter $\delta^{13}C$ values from the Wutongguo Formation range from -21.5 to -24.7‰, resulting in $\Delta^{13}C_{CC\text{-}OM}$ values from 11.1 to 11.2‰. Therefore, although $\delta^{13}C$ values of organic matter from the Moradi Formation are similar to those from contemporaneous sites, Moradi Formation $\Delta^{13}C_{CC\text{-}OM}$ values are larger than contemporaneous sites because of their generally more positive calcite $\delta^{13}C$ values.

3.3. Bone histology

Scapula (MNN MOR148) - Although only half of the scapula is available for sectioning, the bone tissue is very well preserved (Fig. 5A-B). As the result of membrane ossification (Francillon-Vieillot et al., 1990), the scapula is composed of three layers (Fig. 5 A): 1) a slightly compact basal layer of bone; 2) a cancellous core; and 3) an outer compact layer built out by appositional cyclical deposition. In the third layer, five clear LAGs are visible that are regularly spaced out from each other (Fig. 5B). The vascularization is very dense and represented by a longitudinal mesh of primary osteons. Although the collagen matrix is mainly fibrous, some patches of pseudo-lamellar bone are also scarcely distributed over the cortex. The cancellous core exhibits a large amount of radial trabeculae, covered with a secondary lamellar deposit. The basal layer is pierced by numerous, small and simple canals and large primary osteons.

Radius (MNN MOR146) – The radius is a long bone composed of a cortex surrounding a medullary cavity that is secondarily filled with trabeculae (Fig. 5D). These trabeculae form part of the spongiosa. As a result of remodeling (resorption and redeposition), the spongiosa extends to the inner region of the cortex (Fig. 5D). It comprises numerous secondary lamellar trabeculae that are oriented in all directions. The compact cortical bone represents one third of the section area. It is made of fibrous and pseudo-lamellar bone (Fig. 5E, H). In the crest region, some radial extrinsic fibers cut through the bone matrix (Fig. 5E). The bundles of fibers are associated with a dense radial vascular mesh of primary osteons. In the other part of the cortex, the vascularization is composed of longitudinal primary osteons, organized in concentric rows (Fig. 5H). The pareiasaur radius shows a pattern of three LAGs visible in a few places of the compact cortex (Fig. 5G). The distance between these LAGs is constant over the entire thickness of the compacta.

Ulna (MNN MOR147) - The mid-shaft histology of *Bunostegos* ulna exhibits a very densely vascularized cortex. The vascular mesh is made of longitudinal and circular vascular canals and osteons. Based on this great cortical porosity, the spongiosa occupies almost the entire section area. The central part of the

medullary cavity remains free of trabeculae. Because of recrystallization, the bone tissue is too badly preserved to identify any LAG or analyze the bone matrix organization.

Humerus (MNN MOR145) - The surface of the bone has been very much weathered, as a result the compact layer of cortical bone has completely disappeared. The preserved spongiosa has been greatly remodelled and post-mortem recrystallized, and does not preserve to the primary tissue or LAGs. The spongiosa is composed of lamellar and pseudo-lamellar trabeculae, which are relatively loose and evenly distributed in the central region of the section, but denser and slightly organized in concentric rows in the rest of the section.

4. Discussion

This study combines lithological indicators with biological and geochemical proxies of paleoclimate in order to establish a robust reconstruction of terrestrial paleoenvironments. Due to the broad nature of the datasets presented here, they provide a unique insight into climate during Moradi Formation deposition and the extent of seasonality over this region of Pangea.

4.1. Fossil flora

Log - In the area around the excavated log, there were green haloes in the red sediment, as well as mounds of fragmented petrified wood. Though not excavated, each of these occurrences likely represented the presence of a section of a petrified fossil log. Based on the conglomeratic nature of the sediment in which the excavated log was entombed, these logs, taken in toto, may represent a log jam. This means that the 25 m long, possible conifer could have been transported downstream from a wetter upland region.Wood samples from the fossil tree did not show evidence of a seasonal or episodical climate. This could be a preservation artifact, but given its size it is also likely that the root system was able to tap into ground water as its permanent water source.

Taxonomic affiliation - The ovuliferous dwarf shoots of the Moradi conifers have a morphology that is comparable to members of the voltzian Voltziales (or voltzians), a monophyletic group of Paleozoic conifers that includes members of the Majonicaceae (Rothwell et al., 2005). In a phylogenetic analysis by Rothwell et al. (2005) the Permian voltzians were the sister group to the lebachioid walchians, which comprise the other major clade of late-Paleozoic conifer taxa. The ovuliferous cones or fertile zones in these two groups are compound, with bract and dwarf shoots helically arranged along the main axis. The bilaterally symmetrical walchian dwarf shoots consist of more than ten sterile scales with one to three interspersed sporophylls. In contrast to ovuliferous dwarf shoots of walchians, in Late Paleozoic voltzians the basal part of the dwarf-shoot is stalk-like, the vegetative scales and sporophylls are fused at the base and form a flattened structure of distinctly bilateral organization. The vegetative scales and sporophylls are either arranged side by side along the width of the fused structure, or are arranged in two to three planes. In the latter case the sporophylls are always positioned on the adaxial side of the dwarf shoot, with some of the sterile scales forming the abaxial row(s).

The gross morphology of the Moradi dwarf shoots is similar those of members of the Majonicaceae. They have a long stalk, fused bases of vegetative scales and sporophylls, and several vegetative scales positioned on the abaxial side. The only thing reminiscent of walchian dwarf-shoot morphology, is the higher number of scales on the Moradi shoots compared to most voltzian conifer (five or less). This, however, is not a synapomorphy shared by all voltzians, as also the undisputed voltzian *Dolomitia cittertiae* had many sterile scales on the abaxial side of its ovuliferous dwarf-shoots. Therefore, despite their poor conservation, they can be confidently assigned to the voltzian Voltziales. Most voltzian Voltzialean conifers have an irregular orthotropic branching pattern and medium-sized, bifacial ovate to linear leaves (Clement-Westerhof, 1987; Schweitzer, 1963, 1996; Rothwell et al., 2005). So it is quite possible that some of the Moradi leaves were produced by the same plan that produced the ovuliferous dwarf shoots.

Floral biogeographic implications - Before the discovery of the Moradi floras, Permian voltzian conifers were mainly known from Euramerican basins. The oldest known voltzians are found in latest early Permian to early middle Permian deposits from the Midland Basin, north-central Texas, United States (e.g., DiMichele et al., 2001, 2004; Looy 2007, Looy and Stevenson, 2014). Recovered from a channel-form silty deposit, there are in the sub and superjacent strata weakly developed Inceptisols (Tabor and Montañez, 2004; DiMichele et al., 2006; Montañez et al., 2007) and primary gypsum (DiMichele et al., 2001, 2008), suggesting growth on short-lived flood plains in a generally strongly seasonally dry climate. Until now, Lopingian voltzian conifers were exclusively known from seasonally wet plant communities from Europe, particularly from the Zechstein Group of Western Europe and the Val Gardena Sandstone of the Southern Alps (Clement-Westerhof, 1987; Schweitzer, 1986, 1996). The Moradi dwarf shoots show that voltzian conifers were not restricted to arid environments in the equatorial tropics and northern paratropical parts, but instead had a range extending to similar latitudes in the southern hemisphere.

4.2. Stable carbon isotope geochemistry

Soil CO_2 concentrations (C_S; see appendix) estimates from the Moradi Formation (Niger) are the lowest of all Middle and Upper Permian sites; 500 to 1300 ppmV (mean = 800 ±300; Table 3, Appendix). C_S estimates from the Buntsandstein Formation (Italy) range from 1200 to 2800 ppmV (mean = 1800 ±700). The Upper Permian Balfour Fm. samples that conform to 2-component soil CO_2 mixing exhibit a large range of C_S estimates from 800 to 6000 ppmV. The Middle Permian Quanzijie Formation samples provide generally higher and uniform C_S estimates, 6300 ±2600 ppmV.

Differences in soil PCO_2 across a landscape are principally related to differences in soil productivity, which is strongly controlled by the amount of moisture in the soil that is available for floral and microbial metabolic processes (Myers et al., 2012; Tabor et al., 2013; Brook et al., 1983). In this regard, C_S estimates presented herein suggest that the Lopingian soils of the Moradi Formation were among the least productive studied to date. Such low productivity may have been related to more arid conditions, and

increased moisture stress of the Permian soil floras in Niger, compared with other Lopingian paleogeographic sites.

The following equation, modified from Brook and others (1983), relates the concentration of mean growing-season soil CO_2 to actual evapotranspiration:

$$Log\left(\frac{C_S}{10^6}\right) = Log\left(\frac{C_A}{10^6}\right) + 2.09 * (1 - e^{-0.00172 * AET})$$

C_S and C_A are as defined in Eqn 1. AET is actual evapotranspiration in units of mm/yr,, which is the quantity of water that is removed from a surface due to the processes of evaporation and transpiration. If all other factors are held constant, AET will be less in arid climates than in humid climates, because there is less precipitation delivered to the soil to be used in evapotranspiration. Actual evapotranspiration in naturally occurring well-drained soils is almost always less than mean annual precipitation, because some moisture can be lost to through-flow (deep percolation or groundwater) and soil runoff. Therefore, AET estimates effectively provide *minimum* estimates of mean annual precipitation.

Moradi Formation AET estimates are the lowest among all study sites; 110 ±50 mm/yr (Table 2). This is followed, in order of increasing AET estimates, by Buntsandstein (240 ±70 mm/yr), Balfour (320 ±290 mm/yr) and Quanzijie (540 ±110 mm/yr) formations. Thus AET estimates based upon $\delta^{13}C$ values of co-existing calcite and organic matter indicate that the paleogeographic location of the Moradi Fm. was the most arid of Permian sites studied.

In spite of the evidence for aridity garnered from this stable carbon isotope geochemical analysis, the fauna associated with the Moradi formation strata includes large amphibians. This would seem to contradict the geochemistry results. Furthermore, lithological evidence such as shrink-swell features in

paleosol profiles, lateral accretion surfaces in fluvial channels, and non-marine limestones in end-point playa deposits indicate that water was abundant at least intermittently.

Several explanations can account for these different paleo-environmental signals. One possibility is that the paleosols, from which no plant fossils have been recovered, are time equivalent but lateral to the fluvial sediments in the section. This would mean the regional climate was arid with local rivers, and included poorly-drained areas with shallow water tables (cf. DiMichele et al., 2006). Another explanation is that the fluvial sediments represent the wetter times during fluctuating successions of wetter and drier phases. The Moradi sediments were deposited in the continental interior of Pangea, and the Aïr mountains located to the east of the Tim Mersoi Basin would have received additional rainfall due to elevation, but maybe not the massive amounts required to move all the conglomeratic material and other sediments into the lowland. The Moradi flora and fauna could be representative of wetter intervals, and the paleosols that developed during the wetter phases could have either been reworked by the streams or strongly overprinted by the dry phase paleosols.

4.3. Bone histology

The studied pareiasaur bones showed a fibrous matrix and a great density of their vascular network (Fig. 3B, F, and H). This indicates that these individuals had relatively fast bone deposition and active metabolisms. This is in accordance with previous studies, which suggest South-African pareiasaurs experienced rapid growth and short development periods (de Ricqlès, 1978a, b; Canoville and Chinsamy-Turan, 2011).

Although these fossils show evidence of active metabolism, they also exhibit growth marks which are reliable indicators of growth rhythms (Castanet et al., 1993). These growth marks end up as lines of arrested growth (LAGs). In extant tetrapods, LAGs are generally laid down annually (e.g Castanet et al., 1996; Castanet, 1994). The five LAGs counted on the scapula therefore suggest this individual was at

least five years old. The radius must have belonged to an individual older than three years. Since the distance between the LAGs remains constantly large over the period of bone deposition (0.92-1.17 mm between two LAGs at mid-shaft in the radius, Fig. 5G; 1.07-1.71 mm close to the narrowest region of the scapula**,** Fig. 5B), it would seem that the corresponding individuals died while still in development (the LAG interdistance usually decreases with acquisition of sexual maturity; Castanet et al., 2003). This hypothesis regarding the ontogeny of these individuals should be nevertheless tested within the framework of a complete growth-series analysis.

The presence of LAGs in specimens tentatively referred to *Bunostegos* probably results from seasonal or episodic changes in the local climate. The LAG patterns are observed in various individuals, thereby suggesting that these changes must have been contrasted enough to induce successive periods of fast growth and lethargy within this taxon. The regularity of the LAG patterns would evoke a relatively constant succession of seasons. As pareiasaurs have sometimes been considered amphibious (e.g. Kriloff et al., 2008), it is possible that an annual fluctuation in water supply could be one of the major reasons for the cyclical growth patterns inferred here from observations of bone histology.

In each bone where LAG patterns were visible (Fig. 5B, G), bone deposition stopped in the early part of a zone (i.e., when active growth restarted) after the period of dormancy. The time of death is therefore suspected to have occurred during a period when environmental conditions were favorable, i.e., when water was once again available. These observations agree with the taphonomic interpretation of flood events resulting in the accumulation of multiple pareiasaur skeletons.

4.4. The Moradi environment and modern analogues – In places the loessic floodplain silts of the upper Moradi Formation contain discrete shallow roughly circular depressions measuring some 30-50m in diameter filled with a 4-5m thick succession of thinly-bedded lacustrine limestone (Facies C, Fig. 1). At the base of each sequence is a relatively thick and distinctive chaotic limestone “biscuit” breccia filling

deep elongate troughs. The biscuits are platy clasts of reworked calcareous mudstone that appear to have been ripped up from the desiccated mudflats around the lake margins and rapidly dumped into channels cut into the lake bed. Overlying the basal breccia is a succession of thinly bedded and finely laminated carbonate mudstones that display 5-7 stacked depositional cycles. Each 0.5 m cycle comprises climbing ripple cross-lamination with the topmost ripple forms preserved, grading into horizontal laminated lime rich mudstone and terminating in a claystone veneered paleosurface commonly showing desiccation cracks filled with pale red aeolian silt stone and the preferential preservation of trackways. Such sequences are common in playa lake settings and reflect episodic sediment laden floodwaters entering a ponded water body. Interestingly, the flood sequences are overlain by finely laminated mudstone terminating in massive micrite with wrinkle marks and pustular algal-matted patches with desiccation cracks. The superposition of these deep water lacustrine facies on their marginal facies indicates that upper Moradi playa lakes enlarged and deepened over time. A very similar association of edgewise limestone biscuit breccias overlain by turbidite sequences recording decelerating flow, as well as in-situ reed stems, has been recorded in Pleistocene end-point playa deposits of the Namib desert (Smith and Mason, 1998). The classic modern example of this environment is in the hyperarid central Namib Desert where the Sossus river terminates in a dune-dammed playa lake at Sossusvlei.

Paleosol and biotic data from the Moradi Formation give seemingly contradictory results about paleoclimate. Although the paleosol types found in the Moradi (Protosols (similar to Aridisols, Inceptisols, and Entisols) Calcisols, and Vertisols indicate that the prevailing climate was semi- to very arid with pronounced seasonality, there is also sedimentological evidence that these same areas experienced intervals of great water abundance (Tabor et al., 2011; Smith et al., 2015; this paper). Possible present-day analogues for conditions interpreted from the Niger Permian paleosol data, are found in the deserts that are among the driest in the world (Goudie, 2010; Nanson et al., 1992): the Lake Eyre Basin, Central Australia and the Namib Desert, southwestern Africa. Heinrich Walter (Walter, 1984) classified the present global climate zones in zonobiomes (regions defined by particular climates and

ecologies) and orobiomes (biomes located in mountain regions). Both the Namib Desert and Lake Eyre Basin are classified as zonobiome 3: hot, arid subtropical deserts (Breckle, 2002).

The Lake Eyre Basin of central Australia is a barren wasteland of salt plains and sand dunes most years. About twice in every hundred years, the landscape is transformed as heavy rains in the northeast fill the tributary rivers and flood the basin, creating an inland sea (McMahon et al., 2008; Serventy, 1985). While this flooded state occurs infrequently, there are more frequent periods of short small-scale flooding, which fill dry creek beds and temporarily bring life to the floodplains surrounding the lake (Bonython and Mason, 1953). Despite the extremely variable environmental conditions, life thrives in the Lake Eyre Basin. The plants there have morphological and physiological features that permit them to survive prolonged periods of drought, such as persistent seed banks and root systems that penetrate both wide and deep into the soil (Bowman, 2002). Shady groves of large eucalyptus trees provide shelter for large mammals and reptiles, and amphibians (Cockerham, 2004; Serventy, 1985). Such communities can weather the inevitable periods of drought by tapping into deeper water tables, despite being highly saline and saturated in carbonates (Gregory, 1906).

The central and inland regions of the Namib Desert lack the fog belts that somewhat mitigate the dry conditions in the coastal regions. Away from the shore, the greatest amount of vegetation exists in interdune areas, with the greatest diversity in the east (Seely and Ward, 1989). The Kuiseb River course winds through the dunes and escarpments, creating linear ground-water dependent oases that support pockets of desert life. Acacia trees form woodland regions that provide habitats for populations of a wide variety of animals (Seely and Ward, 1989). As evidenced by both the Lake Eyre Basin and the Namib Desert, despite being surrounded by a generally arid climate, even small areas with increased water availability can sustain a wide range of flora and fauna, including large vertebrates and trees. Thus, finding fossil amphibians in the Moradi Formation, i.e. non-amniotic vertebrates that need water at

least for their reproduction, is not so strange when the dynamics revealed by modern analogues are taken into consideration.

5. Conclusions

Description Moradi ecosystem - In sum, we have organisms that lack an amniotic egg and therefore depend on water for reproduction (temnospondyl amphibians), paleosols indicating semi-arid conditions (Tabor et al., 2011), carbon stable isotope data from paleosols indicating arid climatic conditions, and evidence of tall, robust plant life. All of these facts combined suggest that the Permian Moradi Formation was deposited under a generally arid climate that experienced cyclical intermittent periods of water abundance, a place of extreme seasonality or episodicity, supporting what was probably a well-established ground water dependent ecosystem. During the drier, probably longer intervals, we suggest that the Moradi ecosystem was a large arid and relatively flat plain with a sparse plant cover adapted to shallow ground water resources and temporary water ponds in which rare temnospondyl amphibians survived. During the shorter but intense wet intervals, this ecosystem was cut and drained by temporary meandering systems occasionally filled by locally catastrophic flash floods (Smith et al., 2009, 2015).

Acknowledgements

We are indebted to the Nigerien Ministry of Higher Education, Research, and Technology, the National Museum of Niger, and the University of Niamey for supporting our research. We thank T. Smiley, S. Thomas, A. Dindine, A. Maga and B. Tahirou for assistance in the field. N.J. Tabor thanks Francesco Massari (Padova University) for introducing and leading him through the late Permian strata of Italy. S. Streyer and S. Sanchez acknowledge M. Lemoine (MNHN, Paris) for making the bone thin sections. C. Looy thanks I. Poole for making the wood thin sections. W.A. DiMichele and S. Finnegan are thanked for proof reading the draft manuscript. Two anonymous reviewers provided thoughtful and critical reviews, which greatly improved the paper. This project was supported by the National Science Foundation grants EAR 0617250 to N.J. Tabor and EAR-0617718 to C.A. Sidor. S. Sanchez was funded by ERC Advanced

Investigator Grant 233111 (to P. E. Ahlberg), and S.L. Ranks work was funded by the Hellman Foundation (to C.V. Looy). This is University of California Museum of Paleontology Contribution No. xxx.

References

Angielczyk, K.D., Steyer, J.S., Sidor, C.A., Smith, R.M.H., Whatley, R.L., Tolan, S., 2013. Permian and Triassic dicynodont (Therapsida: Anomodontia) faunas of the Luangwa Basin, Zambia: taxonomic update and implications for dicynodont biogeography and biostratigraphy, in: Kammerer, C.F., Angielczyk, K.D., Fröbisch, J. (Eds.), The early evolutionary history of Synapsida. Springer, Dordrecht, pp. 93–138

Blodgett, R.H., 1988. Calcareous paleosols in the Triassic Dolores Formation, southwestern Colorado. Geol. S. Am. S. 216, 103–121.

Bonython, C.W., Mason, B., 1953. The filling and drying of Lake Eyre. Geogr. J. 119, 321–330.

Boutton, T.W., 1991. Stable carbon isotope ratios of natural materials: II. Atmospheric, terrestrial, marine and freshwater environments, in: Coleman, D.C., Fry, B. (Eds.), Carbon Isotope Techniques. Academic Press, San Diego, pp. 155–170.

Bowman, D.M.J.S., 2002. The Australian summer monsoon: a biogeographic perspective. Aust. Geogr. Stud. 40, 261–277.

Breckle, S.-W., 2002. Walter's vegetation of the earth: the ecological systems of the geo-biosphere, Springer, Berlin.

Brook, G.A., Folkoff, M.E., Box, E.O., 1983. A world model of soil carbon dioxide. Earth Surf. Proc. Land. 8, 79–88.

Canoville, A., Chinsamy-Turan, A., 2011. Growth patterns and palaeoecology of pareiasaurs (parareptilia, pareiasauridae) inferred from long bone histology and microanatomy. J. Vertebr. Paleontol. 31 (Suppl. 3), 83.

Castanet, J., 1994. Age estimation and longevity in Reptiles. Gerontology 40, 174–192.

Castanet, J., Baez, M., 1991. Adaptation and evolution in *Gallotia* lizards from the Canary Islands: age, growth, maturity and longevity. Amphibia-Reptilia 12, 81–102.

Castanet, J., Francillon-Vieillot, H., Bruce, R.C., 1996. Age estimation in desmognathine salamanders assessed by skeletochronology. Herpetologica 52, 160–171.

Castanet, J., Francillon-Vieillot, H., Meunier, F.-J., de Ricqlès, A., 1993. Bone and individual aging, in: Hall, B.K. (Ed.), Bone Vol. 7: Bone Growth-B. CRC Press, Boca Raton, pp. 245–283.

Castanet, J., Francillon-Vieillot, H., de Ricqlès, A., 2003. The skeletal histology of the Amphibia, in: Heatwole, H., Davies, M. (Eds.), Amphibian Biology, Vol. 5: Osteology. Surrey Beatty & Sons, Chipping Norton, pp. 1598–1683.

Clement-Westerhof, J.A., 1987. Aspects of Permian palaeobotany and palynology. VII. The Majonicaceae, a new family of Late Permian conifers. Rev. Palaeobot. Palynol. 52, 375–402.

Cockerham, S.T., 2004. Irrigation and planting density affect river red gum growth. Calif. Agr. 58, 40–43.

Craig, H., 1957, Isotopic standards for carbon and oxygen and correction factors for mass-spectrometric analysis of carbon dioxide: Geochim. Cosmochim. Acta 12, 133–149.

Damiani, R.O., Sidor, C.A., Steyer, J.-S., Smith, R.M.H., O'Keefe, F.R., Larsson, H.C.E., Maga, A., Ide, O., 2006. The vertebrate fauna of the Upper Permian of Niger. V. The primitive temnospondyl *Saharastega moradiensisi*. J. Vertebr. Paleontol. 26, 559–572.

de Ricqlès, A., 1981. Recherches paléohistologiques sur les os longs des tétrapodes. VI—Les Stégocéphales. Ann. Paléontol. 67, 141–157.

de Ricqlès, A., 1978a. Recherches paléohistologiques sur les os longs des tétrapodes. VII—Sur la classification, la signification fonctionnelle et l'histoire des tissus osseux des tétrapodes (Troisième partie: Evolution: considérations phylogénétiques). Ann. Paléontol. 64, 85–111.

de Ricqlès, A., 1978b. Recherches paléohistologiques sur les os longs des tétrapodes. VII—Sur la classification, la signification fonctionnelle et l'histoire des tissus osseux des tétrapodes (Troisième partie: Les problèmes du déterminisme des types de tissus osseux). Ann. Paléontol. 64, 153–184.

de Ricqlès, A., 1975. Recherches paléohistologiques sur les os longs des tétrapodes. VII—Sur la classification, la signification fonctionnelle et l'histoire des tissus osseux des tétrapodes (Première partie: Structures). Ann. Paléontol. 61, 49–129.

de Ricqlès, A., Castanet, J., Francillon-Vieillot, H., 2004. The 'message' of bone tissue in paleoherpetology. Ital. J. Zool. 71 S2, 3–12.

de Ricqlès, A., Taquet, P., 1982. La faune de vertébrés du Permien Supérieur du Niger.—I. Le captorhinomorphe *Moradisaurus grandis* (Reptilia, Cotylosauria). Ann. Paléontol. 68, 33–106.

DiMichele, W.A., Hook, R.W., Nelson, W.J., Chaney, D.S., 2004 An unusual Middle Permian flora from the Blaine Formation (Pease River Group, Leonardian-Guadalupian Series) of King County, west Texas. J. Paleontol. 78, 765–782.

DiMichele, W.A., Mamay, S.H., Chaney, D.S., Hook, R.W., 2001. An Early Permian flora with Late Permian and Mesozoic affinities from north-central Texas. J. Paleontol. 75, 449–460.

DiMichele, W.A., Tabor, N.J., Chaney, D.S., Nelson, W.J., 2006. From wetlands to wet spots: environmental tracking and the fate of Carboniferous elements in Early Permian tropical floras, in: Greb, S.F., DiMichele, W.A. (Eds.), Wetlands through time. Geol. S. Am. S. 399, 223–248.

DiMichele, W.A., Kerp, H., Tabor, N.J., Looy, C.V., 2008. The so-called "Paleophytic–Mesophytic" transition in equatorial Pangea—Multiple biomes and vegetational tracking of climate change through geological time. Palaeogeogr. Palaeoclimatol. Palaeoecol. 268, 152–163.

Fielding, C.R., Alexander, J., 2001. Fossil trees in ancient fluvial channel deposits: evidence of seasonal and longer-term climatic stability. Palaeogeogr. Palaeoclimatol. Palaeoecol. 170, 59–80.

Fluteau, F., Besse, J., Broutin, J. Ramstein, G. 2001. The Late Permian climate. What can be inferred from climate modelling concerning Pangea scenarios and Hercynian range altitude? Palaeogeogr. Palaeoclimatol. Palaeoecol. 167, 39–71.

Francillon-Vieillot, H., de Buffrénil, V., Castanet, J., Géraudie, J., Meunier, F.-J., Sire, J.-Y., Zylberberg, L., de Ricqlès, A., 1990. Microstructure and mineralization of vertebrate skeletal tissues, in: Carter, J.G. (Ed.), Skeletal biomineralization: patterns, processes and evolutionary trends. American Geophysical Union, San Francisco, 175–234.

Gastaldo, R.A., Demko, T.M., 2010. The relationship between continental landscape evolution and the plant-fossil record: long term hydrologic controls on preservation, in: Allison, P.A., Bottjer, D.J. (Eds.), Taphonomy. Process and Bias Through Time. Top. Geobiol. 32, 250–285.

Gastaldo, R.A., Pludow, B.A., Neveling, J., 2013, Mud aggregates from the Katberg Formation, South Africa: Additional evidence for Early Triassic degradational landscapes. J. Sediment. Res. 83, 531–540.

Gastaldo, R.A., Knight, C., Neveling, J., Tabor, N., 2014. Late Permian Paleosols from Wapadsberg Pass, South Africa: Implications for Changhsingian Climate. Geo. Soc. Am. Bull. 126, 665–679.

Germain, D., 2010. The Moroccan diplocaulid: the last lepospondyl, the single one on Gondwana. Hist. Biol. 22, 4–39.

Gibbs, M.T., Rees, P.M., Kutzbach, J.E., Ziegler, A.M., Behling, P.J., Rowley, D.B., 2002. Simulations of Permian climate and comparisons with climate sensitive sediments. J. Geol. 110, 33–55.

Giles, M.J., Soregham, M.J., Benison, K.C., Soregham, G.S., Hasiotis, S.T., 2013. Lakes, loess and paleosols in the Permian Wellington Formation of Oklahoma, USA: Implications for paleoclimate and paleogeography of the mid-continent. J. Sedimentary Res. 83, 825-846.

Goudie, A., 2010. Namib sand sea: large dunes in an ancient desert, in: Migon, P. (Ed), Geomorphological Landscapes of the World. Springer, Netherlands, 163–169.

Gregory, J.W., 1906. The dead heart of Australia: A journey around Lake Eyre in the summer of 1901-1902, with some account of the Lake Eyre basin and the flowing wells of central Australia. John Murray, London.

Hass, H., Rowe, N.P., 1999. Thin sections and wafering, in: Jones, T.P., Rowe, N.P. (Eds.), Fossil plants and spores: modern techniques. The Geological Society, London, 76–81.

Hernandez-Castillo, G.R., Rothwell, G.W., Mapes, G., 2001. Thucydiaceae fam. nov., with a review and reevaluation of Paleozoic walchian conifers. Int. J. Plant. Sci. 162, 1155–1185.

Jalil, N.E., Dutuit, J.M., 1996. Permian captorhinid reptiles from the Argana Formation, Morocco. Palaeontology 39, 907–918.

Jalil, N.E., Janvier, P., 2005. Les pareiasaures (Amniota, Parareptilia) du Permien supérieur du Bassin d'Argana, Maroc. Geodiversitas 27, 35–132.

Kiehl, J.T., Shields, C.A., 2005. Climate simulation of the latest Permian: Implications for mass extinction. Geology 33, 757–760.

Klappa, C.F., 1980. Rhizoliths in terrestrial carbonates: classification, recognition, genesis and significance. Sedimentology 27, 613–629.

Köhler, M., Marín-Moratalla, N., Jordana, X., Aanes, R., 2012. Seasonal bone growth and physiology in endotherms shed light on dinosaur physiology. Nature 487, 358–361.

Konietzko-Meier, D., Klein, N., 2013. Unique growth pattern of Metoposaurus diagnosticus krasiejowensis (Amphibia, Temnospondyli) from the Upper Triassic of Krasiejów, Poland. Palaeogeogr. Palaeoclimatol. Palaeoecol. 370, 145–157.

Kriloff, A., Germain, D., Canoville, P., Vincent, P., Sache, M., Laurin, M., 2008. Evolution of bone microanatomy of the tetrapod tibia and its use in palaeobiological inference. J. Evolution. Biol. 21, 807–826.

Lamm, E.-T., 2013. Preparation and sectioning of specimens, in: Padian, K., Lamm, E.-T. (Eds.), Bone histology of fossil tetrapods. University of California Press, Berkeley, 55-160.

Looy, C.V., 2007. Extending the range of derived Late Paleozoic conifers: *Lebowskia* gen. nov. (Majonicaceae). Int. J. Plant Sci. 168, 957–972.

Looy, C.V., Stevenson, R.A., 2014. Earliest occurrence of autorotating seeds in conifers: the Permian (Kungurian-Roadian) *Manifera talaris* gen. et sp. nov. Int. J. Plant Sci. 175, 841–854.

Lucas, S.G., 2004. A global hiatus in the Middle Permian tetrapod fossil record. Stratigraphy 1, 47–64.

Machette, M.N., 1985. Calcic soils of the southwestern United States, in: Wiede, D.L. (Ed.), Soils and Quaternary Geology of the Southwestern United States, Geological Society of America Special Paper 203, 1-22.

McMahon, T.A., Murphy, R.E., Peel, M.C., Costelloe, J.F., Chiew, F.H.S., 2008. Understanding the surface hydrology of the Lake Eyre Basin: Part 1—Rainfall. J. Arid Environ. 72, 1853–1868.

Montañez, I.P., Tabor, N.J.,Niemeier, D., DiMichele,W.A., Frank, T.D., Fielding, C.R., Isbell, J.L., 2007. CO_2-forced climate and vegetation instability during Late Paleozoic deglaciation. Science 315, 87–91.

Myers, T.S., Tabor, N.J., Jacobs, L.L., Mateus, O., 2012, Estimating soil pCO_2 using paleosol carbonates: implications for the relationship between primary productivity and faunal richness in ancient terrestrial ecosystems. Paleobiology 38, 585–604.

Nanson, G.C., Price, D.M., Short, S.A., 1992. Wetting and drying of Australia over the past 300 ka. Geology 20, 791–794.

O'Keefe, F.R., Sidor, C.A., Larsson, H.C.E., Maga, A., Ide, O., 2005. The vertebrate fauna of the Upper Permian of Niger—III, Morphology and ontogeny of the hindlimb of *Moradisaurus grandis* (Reptilia, Captorhinidae). J. Vertebr. Paleontol. 25, 309–319.

Peyser, C.E., Poulsen, C.J., 2008. Controls on Permo-Carboniferous precipitation over tropical Pangaea: a GCM sensitivity study. Palaeogeogr. Palaeoclimatol. Palaeoecol. 268, 181–192.

Philippe, M., Bamford, M.K., 2008. A key to morphogenera used for Mesozoic conifer-like woods. Rev. Palaeobot. Palyno. 148, 184–207.

Rees, P.M., Ziegler, A.M., Gibbs, M.T., Kutzbach, J.E., Behling, P.J., Rowley, D.B., 2002. Permian phytogeographic patterns and climate data/model comparisons. J. Geol. 110, 1–31.

Rothwell GW, Mapes, G., Hernandez-Castillo, G.R., 2005 *Hanskerpia* gen. nov. and phylogenetic relationships among the most ancient conifers (Voltziales). Taxon 54, 733–750.

Sanchez, S., Schoch, R.R., 2013. Bone histology reveals a high environmental and metabolic plasticity as a successful evolutionary strategy in a long-lived homeostatic Triassic temnospondyl. Evol. Biol. 40, 627–647.

Sanchez, S., Klembara, J., Castanet, J., Steyer, J.-S., 2008. Salamander-like development in a seymouriamorph revealed by palaeohistology. Biol. Letters 4, 411–414.

Sanchez, S., Schoch, R.R., de Ricqlès, A., Steyer, J.-S., 2010a. Palaeoecological and palaeoenvironmental influences revealed by long-bone palaeohistology: the example of the Permian branchiosaurid *Apateon*, in: Vecoli, M., Clement, G., Meyer Berthaud, B. (Eds.), The terrestrialization process: modelling complex interactions at the biosphere-geosphere Interface. Geol. Soc. Spec. Publ. 339, 139–149.

Sanchez, S., de Ricqlès, A., Schoch, R.R., Steyer J.-S., 2010b. Developmental plasticity of limb bone microstructural organization in *Apateon*: histological evidence of paedomorphic conditions in branchiosaurs. Evol. Dev. 12, 315–328.

Scheyer, T.M., Sander, P.M., 2009. Bone microstructures and mode of skeletogenesis in osteoderms of three pareiasaur taxa from the Permian of South Africa. J. Evolution. Biol. 22, 1153–1162.

Schweitzer, H.J., 1963. Der weibliche Zapfen von *Pseudovoltzia liebeana* and seine Bedeutung für die Phylogenie der Koniferen. Palaeontogr. Abt. B 113, 1–29.

Schweitzer, H.J., 1986. The land flora of the English and German Zechstein sequences, in: Harwood, G.M, Smith. D.B. (Eds.), The English Zechstein and related topics. Geological Society Special Publication 22. Geological Society-Blackwell Scientific, Oxford, 31–54.

Schweitzer, H.J., 1996 *Voltzia hexagona* (Bischoff) Geinitz aus dem mittleren Perm Westdeutschlands. Palaeontogr. Abt. B 293, 1–22.

Scotese, C.R., Boucot, A.J., McKerrow, W.S., 1999. Gondwanan palaeogeography and palaeoclimatology. J. Afr. Earth Sci. 28, 99–114.

Seely M.K., Ward, J.D., 1989. Ecological aspects of dunes in the central Namib Desert. Dunes '89 excursion 2A field guide, Desert Ecological Research Unit, Gobabeb.

Semeniuk, V., 1981. Calcrete in Quaternary coastal dunes in southwestern Australia: a capillary-rise phenomenon associated with plants. J. Sediment. Petrol. 51, 47–68.

Semeniuk, V., 1985. Distribution of calcrete in Holocene coastal sands in relationship to climate, southwestern Australia. J. Sediment. Petrol. 55, 86–95.

Serventy, V., 1985. The desert sea. The miracle of Lake Eyre in flood. MacMillan Company of Australia, Melbourne.

Sidor, C.A., 2013. The vertebrate fauna of the Upper Permian of Niger—VIII. *Nigerpeton ricqlesi* (Temnospondyli: Cochleosauridae) and tetrapod biogeographic provinces. C. R. Palevol. 12, 463–472.

Sidor, C.A., Blackburn, D.C., Gado, B., 2003. The vertebrate fauna of the Upper Permian of Niger—II. Preliminary description of a new pareiasaur. Palaeontol. Afr. 39, 42–52.

Sidor, C.A., O'Keefe, F.R., Damiani, R., Steyer, J.S., Smith, R.M.H., Larson, H.C.E., Sereno, P.C., Ide, O., Maga, A., 2005. Permian tetrapods from the Sahara show climate-controlled endemism in Pangea. Nature 434, 886–889.

Sidor, C.A., Vilhena, D.A., Angielczyk, K.D., Huttenlocker, A.K., Nesbitt, S.J., Peecook, B.R., Steyer, J.S., Smith, R.M.H., Tsuji, L.A.. 2013. Provincialization of terrestrial faunas following the end-Permian mass extinction. P. Natl. Acad. Sci. USA 110, 8129–8133.

Smiley, T.M., Sidor, C.A., Maga, A., Ide, O., 2008. The vertebrate fauna of the Upper Permian of Niger. —VI. First evidence of a gorgonopsian therapsid. J. Vertebr. Paleontol. 28, 543–547.

Smith, R.M.H., Mason, T.R., 1998. Sedimentary Environments and Trace Fossils of Tertiary Oasis Deposits in the Central Namib Desert, Namibia. Palaios 13, 547–559.

Smith, R.M.H., Sidor, C.A., Tabor, N.J., Steyer, J.S., Chaney, D.S., 2009. Vertebrate taphonomy and ichnology of a Permian 'wet desert' in central Pangea. Palaeontol. Africana 44, 179–183.

Smith, R.M.H., Sidor, C.A., Tabor, N.J., Steyer, J.S., 2015. Sedimentology and vertebrate taphonomy of the Moradi Formation of northern Niger: A Permian wet desert in the tropics of Pangaea. Palaeogeogr. Palaeoclimatol. Palaeoecol. 440, 128-141.

Steyer, J.-S., Jalil, N.E., 2009. First evidence of a temnospondyl in the Late Permian of the Argana Basin, Morocco. Spec. Pap. Palaeontol. 81, 155–160.

Steyer, J.-S., Damiani, R., Sidor, C.A., O'Keefe, F.R., Larsson, H.C.E., Maga, A., Ide, O., 2006. The vertebrate fauna of the Upper Permian of Niger. —IV. *Nigerpeton ricqlesi* (Temnospondyli: Cochleosauridae), and the edopoid colonization of Gondwana. J. Vertebr. Paleontol. 26, 18–28.

Steyer, J.-S., Laurin, M., Castanet, J., de Ricqlès, A., 2004. First histological and skeletochronological data on temnospondyl growth: palaeoecological and palaeoclimatological implications. Palaeogeogr. Palaeoclimatol. Palaeoecol. 206, 193–201.

Tabor, N.J., Montañez, I.P., 2004. Permo-Pennsylvanian alluvial paleosols (north-central Texas): High-resolution proxy records of the evolution of early Pangean paleoclimate. Sedimentology 51, 851–884.

Tabor, N.J., Smith, R.M.H., Steyer, S.J., Sidor, C.A., Poulsen, C.J., 2011. The Permian Moradi Formation of northern Niger: Paleosol morphology, petrography and mineralogy. Palaeogeogr. Palaeoclimatol. Palaeoecol. 299, 200–213.

Tabor, N.J., Myers, T.S., Gulbranson, E., Rasmussen, C., Sheldon, N.D., 2013. Light stable isotope composition of modern calcareous soil profiles in California: Implications for CO_2 reconstructions from calcareous paleosols. Soc. Econ. Paleontol. Mineral. Spec. Publ. 104, 17–34.

Taquet, P., 1969. Première découverte en Afrique d'un reptile captorhinomorphe (Cotylosaurien). C. R. Acad. Sci. Ser. D 268, 779–781.

Tooth, S., Nanson, G.C., 2000. The role of vegetation in the Fm. of anabranching channels in an ephemeral river, northern plains, arid central Australia. Hydrol. Process. 14, 3099–3117.

Tsuji, L.A., Sidor, C.A., Steyer, J.-S., Smith, R.M.H., Tabor, N.J., Ide, O., 2013. The vertebrate fauna of the Upper Permian of Niger—VII. Cranial anatomy and relationships of *Bunostegos akokanensis* (Pareiasauria). J. Vertebr. Paleontol. 33, 747–763.

Turner, M.L., Tsuji, L.A., Ide, O., Sidor, C.A., 2015. The vertebrate fauna of the upper Permian of Niger—IX. The appendicular skeleton of *Bunostegos akokanensis* (Parareptilia: Pareiasauria), Journal of Vertebrate Paleontology. http://dx.doi.org/10.1080/02724634.2014.994746

Walter, H., 1984. Vegetation und Klimazonen. Grundriß der globalen Ökologie. Verlag E. Ulmer, Stuttgart.

Watson, A., 1992. Desert soils, in: Martini, I., Chesworth, W. (Eds.), Weathering, Soils and Paleosols. Elsevier, Amsterdam, 225–260.

Wright, V.P., 1990. A micromorphological classification of fossil and recent calcic and petrocalcic microstructures, in: Douglas, L.A. (Ed.), Soil Micromorphology: A Basic and Applied Science. Elsevier, Amsterdam, 401–407.

Yang, W., Feng, Qi., Liu, Y.Q., Tabor, N., Lin, J.Y., Thomas, S., Miggins, D., 2010. Depositional environments and cyclo- and chronostratigraphy of uppermost Carboniferous–Lower Triassic fluvial–lacustrine deposits. Global Planet. Change 73, 15–113.

Figure Captions

Fig. 1. Stratigraphy, depositional facies and fossils of the Late Permian upper Moradi Formation in Northern Niger. A= high sinuosity, gravelly sand bed channel fill; B= loessic floodplain with anastomosed distributary channels; C= end-point lake with exposed carbonate mudflats; D= gravel-bed braided channel fill. **Add info on new part of the figure.**

Fig. 2. Fossil leaves from the Moradi Formation found at localities T09 and T24. Scale bars equal 5 mm. (A) MNN MOR139, narrow strap-like leaves of Morphotype 1. (B) MNN MOR140, wide strap-like leaves of Morphotype 2. Lengthwise striations from thick veins can be seen in the inset. (C) MNN MOR141 and (D) MNN MOR142, needle-like leaves of Morphotype 3. (E) MNN MOR143 and (F) MNN MOR144 are impressions of the obovate leaves of Morphotype 4.

Fig. 3. Ovuliferous conifer dwarf shoots. Scale bars equal 5 mm. (A) MNN MOR114 shows a distinct lobed central scale. (B) MNN MOR115 shows that the scales come in a variety of thicknesses on each individual shoot. (C) MNN MO116 displays the remarkable number of scales an individual shoot can possess. (D) MNN MOR118 is paired with its counterpart (E) to form (F), which is a rare example of how the full dwarf shoot would have looked in cross-section after burial, with a thickness of at least 4 mm (not accounting for desiccation). (G) MNN MOR44 shows a prominent lobed scale on the leftmost side. (H) MNN MOR117, (I) MNN MOR119, and (J) MNN MOR120 are examples of complete dwarf shoots, including stalks. (K) MNN MOR121 shows the point of attachment for two dwarf shoots joined at the base. It is likely that attached dwarf shoots were arranged in groups.

Fig. 4. Diagram of the Moradi tree trunk fossil. Scale bar in the lower left-hand corner of each inset represents 0.5 m. Red circles along the tree trunk diagram show position and size of branch scars. At the base of the trunk, from 0-1.5 m, the remains were badly damaged; likewise from 13.45-14.40 m, the

remains were broken and crumbled. From 23-24 m, the trunk was mostly buried. Likewise, past 25 m the trunk was not excavated.

Fig. 5. Histology of isolated pareiasaur bones from the Moradi Formation, Upper Permian of Niger.(A) Thin section, made from a scapula (MNN MOR148; ordinary transmitted light), displaying three layers: the basal layer (bl), the cancellous core (cc) and the outer layer (ol). (B) Detail of the region framed in A (polarized light). The red arrows show the regular pattern of lines of arrested growth (LAGs). (C) Radius (MNN MOR146) as preserved. The black arrow indicates the location where the thin section was made at mid-shaft. (D) Mid-shaft thin section of radius showing the compact cortical bone (c) and the spongiosa (s) (ordinary transmitted light). The frames, displayed from top to bottom, correspond to the images E-H. (E) Detail of the compact cortex (polarized light) showing a region of rearrangement with radial extrinsic fibers oriented in the same axis as the vascular mesh (vc). The primary bone tissue shows patches of pseudo-lamellar bone (plb). (F) Detail of the compact cortex displaying the organization of primary osteons (po) and the fibrous primary bone matrix (fb) in the same region as E (polarized light). (G) Detail of another region of compact cortical bone showing a regular LAG pattern (ordinary transmitted light). LAGs are highlighted by the red arrows. (H) Fibrous bone matrix (fb) pierced by circumferential rows of primary osteons (po) (polarized light).

Table 1. Sample information for carbonates analyzed from the Moradi, Quanzijie, Wutonggou, Balfour, Buntsandstein Formations.

Table 2. Sample information and stable carbon isotope values for calcite ($\Delta^{13}C_{CC}$) and organic matter $\delta^{13}C_{OM}$) as well as estimates of Soil PCO_2 (in ppmV) and actual evapotranspiration (AET) from the Moradi, Quanzijie, Wutonggou, Balfour, Buntsandstein Formations.

Appendix

CO_2 mixing in soils - Soils may be characterized by mixing of one, two, or three components of soil CO_2, which can result in significantly different $\delta^{13}C$ values of soil CO_2 and the resulting pedogenic calcite (Tabor et al., 2013; Sheldon and Tabor, 2009; Feng and Yapp, 2009; Tabor and Yapp, 2005; Yapp, 2002; Hsieh and Yapp, 1999). The three CO_2 components are derived from (1) oxidation of *in situ* organic matter, (2) tropospheric CO_2, and (3) dissolution of pre-existing carbon-bearing minerals such as calcite in the soil.. None of the paleosols from the Moradi Formation or other sites in China, South Africa and Italy are stratigraphically associated with marine or lacustrine limestone strata. Therefore, the following discussion considers only 1- and 2-component mixing of soil CO_2 as viable explanations for carbon isotope data collected from Middle and Upper Permian paleosols.

Soils characterized by one component of CO_2 form under a chemically closed or semi-closed system (e.g. Tabor et al., 2013; Tabor et al., 2007; Gluyas, 1984; Sheldon and Tabor, 2009) that arises in settings where gaseous diffusion between the soil and the troposphere is limited, usually as a result of poorly drained, waterlogged conditions within the soil profile. Diffusion from the troposphere (including CO_2) to the wet soil is limited, and aqueous O_2 in the soil is quickly consumed by the oxidation of organic matter (Feng and Hsieh, 1998). Under these conditions, both bicarbonate and calcite will have $\delta^{13}C$ values that are equivalent to that of the oxidizing organic matter in the closed-system soil. Soil profiles forming under semi-closed conditions will result in calcite $\delta^{13}C$ values that are less than 14.6‰ more positive than coexisting organic matter (at 20° C), which reflects the diffusive 4.4‰ enrichment in $\delta^{13}C$ in the biologically-derived CO_2 (Cerling et al., 1991), as well as an additional 10.2‰ carbon isotope enrichment from gaseous CO_2 to calcite due to carbon isotope fractionation between carbonate species (at mildly alkaline pH; Romanek et al., 1992) in open system 2-component CO_2 mixing.

For example, both samples (n = 2) from the Upper Permian Wutonggou Formation and over half (n = 3) of the samples from the Upper Permian Balfour Formation have $\delta^{13}C_{m(CC)}$ values that are less than 14.6‰ more positive than co-existing $\delta^{13}C_{OM}$ values, and therefore do not permit meaningful estimates of Soil CO_2 concentrations ($C_{S;}$ Table 2). The paleosols of the Balfour Formation exhibit drab matrix colors, little to no soil structure, as well as pyrite and gypsum crystals and are interpreted to have been formed in swampy bottomlands (Gastaldo et al., 2009; 2014; Tabor et al., 2007; Retallack et al., 2003). Upper Permian Wutonggou paleosols have drab matrix colors, iron and manganese concretions, and are interpreted to have formed on a poorly-drained lake plain (Yang et al., 2007; Thomas et al., 2010). The results from these five samples were therefore interpreted to reflect calcite crystallization in a closed or semi-closed system dominated by one component of CO_2 derived from oxidation of in-situ organic matter, and are not considered further. All other Middle and Upper Permian samples have $\delta^{13}C_{m(CC)}$ and $\delta^{13}C_{OM}$ values consistent with formation in a soil characterized by mixing of two components of CO_2, and therefore may provide information about variations in soil PCO_2 (C_S) among those sites.

Soils characterized by two-component soil CO_2 mixing assumes that the only two sources contributing to soil CO_2 are CO_2 from the open atmosphere (tropospheric CO_2) and CO_2 from *in situ* oxidation of biological carbon in the soil. Steady-state solutions to the one-dimensional Fickian diffusion equation yield reasonable representations of $\delta^{13}C$ values of soil CO_2 with depth in modern soils characterized by mixing of two sources of CO_2 (Cerling, 1984). In these models, PCO_2 and $\delta^{13}C$ values of Earth's atmosphere are the upper boundary conditions, and there is a depth-dependent CO_2 production term that describes the oxidation of organic carbon in the soil. Above a characteristic CO_2 production depth within the soil, both the concentration and $\delta^{13}C$ of soil CO_2 will progressively approach values of the Earth's atmosphere. The characteristic production depth in carbonate-forming soils varies, but tends to be at least 300-500 mm beneath the soil surface (Breecker et al., 2009; Cerling and Quade, 1993; Quade et al., 1989). It is important to note that calcite samples from all paleosols considered herein were collected from at least 500 mm beneath the interpreted surface of the paleosol profile, and therefore calcite $\delta^{13}C$

values should reflect the maximum contribution of CO_2 from oxidation of organic matter, and provide maximum soil PCO_2 (C_S) estimates. Thus, CO_2 in soil gas can be generally regarded as a mixture of two isotopically distinct end-members in these soils: atmospheric CO_2 and CO_2 derived from *in-situ* oxidation of soil organic matter. Calcite $\delta^{13}C$ values that are ≥14.6‰ more positive than co-existing oxidizing organic matter reflect proportionately larger contributions from isotopically lighter atmospheric CO_2 to the soil atmosphere.

Permian Soil CO_2 estimates - Although its potential has been largely ignored to date (however, see Yapp and Poths, 1996; Sheldon and Tabor, 2009; Myers et al., 2012), paleosol calcite $\delta^{13}C$ values may be tremendously useful as a proxy of soil PCO_2 and biological productivity for times prior to the evolution of C_4 plants and their rise to dominance in some ecosystems (pre-Miocene time). The following equation relates measured calcite and organic matter $\delta^{13}C$ values to soil PCO_2 estimates:

$$C_{S(cc)} = C_{A(cc)} * \frac{d^{13}C_{A(cc)} - d^{13}C_{O(cc)}}{d^{13}C_{m(CC)} - d^{13}C_{O(cc)}}.$$

The subscript "(cc)" indicates calcite. $d^{13}C_{m_{(cc)}}$ is the measured $\delta^{13}C$ value of pedogenic calcite ($\delta^{13}C_{CC}$ in Table 2). The $\delta^{13}C$ values subscripted with "A" and "O" are the $\delta^{13}C$ values of calcite formed solely in equilibrium with CO_2 derived from the atmosphere and from oxidation of soil organic matter, respectively. C_A refers to the concentration of CO_2 gas in the soil if the only contribution to soil CO_2 were from the atmosphere. C_S is the actual concentration of CO_2 that was present in the soil. Both C_A and C_S are in units of ppmV. The value for ($d^{13}C_{A_{(cc)}} - d^{13}C_{O_{(cc)}}$) is assumed to be +16‰ (Yapp and Poths, 1991, 1992, 1993, 1996), because it represents the approximate difference between the estimated $\delta^{13}C$ values of pre-industrial atmospheric CO_2 (–6.5‰) and recent C_3 continental biota (–27‰), after the latter value is adjusted for the diffusive 4.4 ‰ enrichment in $\delta^{13}C$ in the biologically-derived CO_2 of the soil (Cerling et

al., 1991). Note that other ($\delta^{13}C_{A_{(cc)}} - \delta^{13}C_{O_{(cc)}}$) values have been suggested (e.g. ~13.7‰, Arens et al., 2000), but differences in this quantity result in relatively minor differences in estimated pCO_2 values (Sheldon and Tabor, 2009; Tabor et al., 2004; Yapp and Poths, 1991).

$\delta^{13}C_{O(cc)}$ values may be estimated from $\delta^{13}C$ values of co-existing organic matter within the paleosol profiles (Montañez et al., 2007; Tabor et al., 2004; Yapp and Poths, 1996; $\delta^{13}C_{OM}$ in Table 2). $\delta^{13}C_{O(cc)}$ estimates are 14.6‰ heavier than $\delta^{13}C$ values of organic matter, which reflects the diffusive 4.4‰ enrichment in $\delta^{13}C$ in the biologically-derived CO_2 (Cerling et al., 1991), as well as an additional 10.2‰ carbon isotope enrichment from gaseous CO_2 to calcite due to carbon isotope fractionation between carbonate species (at mildly alkaline pH and 20° C; Romanek et al., 1992). If $\delta^{13}C_{O(cc)}$ estimates are more positive than $\delta^{13}C_{m(CC)}$ values from the same paleosol, C_S estimates will have a negative value. As discussed earlier, negative C_S values have no physical meaning, and rather reflect that either (1) calcite crystallization occurred in a chemically closed or semi-closed system or (2) the organic matter and calcite $\delta^{13}C$ values do not share a common pedogenic origin.

C_A values are not known with certainty for Middle and Late Permian time. Estimates for Middle and Late Permian paleoatmospheric PCO_2 range from ~PAL (Present Atmospheric Level; ~300 ppmV) to ~17 x PAL (e.g. Berner, 2005; Royer et al., 2004; Retallack, 2002). However, it is not necessary to know C_A explicitly. This reflects the fact that the troposphere is a well-mixed system (e.g. Cerling, 1984), so for any given interval of time in earth history, C_A will be effectively equivalent at all places upon Earth's surface. Therefore, a comparative analysis of paleosol calcite and organic matter from penecontemporaneous sites should delineate differences in C_S, as related to variations in biologically-produced CO_2, since C_A would have been equivalent among all sites considered. With respect to these aforementioned considerations, it was assumed that all paleosol samples (1) are penecontemporaneous (with respect to significant temporal changes in C_A values) and (2) formed in the presence of a constant

atmospheric PCO_2 (C_A) value of 300 ppmV. Note that this assumed C_A value will result in relatively low C_S estimates, and that higher C_A values will produce correspondingly higher estimates of C_S (Sheldon and Tabor, 2009; Tabor et al., 2013).

Citations for the Appendix

Arens, N.C., Jahren, A.H., Amundson, R., 2000. Can C3 plants faithfully record the carbon isotopic composition of atmospheric carbon dioxide? Paleobiology 26, 134–164.

Berner, R.A., 2005. GEOCARBSULF: A combined model for phanerozoic atmospheric O_2. Geochimica et Cosmochimica. Acta 70, 5653–5664.

Breecker, D.O., Sharp, Z.D., McFadden, L.D., 2009. Seasonal bias in the formation and stable isotopic of pedogenic carbonate in modern soils from central New Mexico, USA. Geological Society of America Bulletin 121, 630–640.

Cerling, T.E., 1984. The stable isotopic composition of modern soil carbonate and its relationship to climate. Earth and Planetary Science Letters 71, 229–240.

Cerling, T.E., Quade, J., 1993. Stable carbon and oxygen isotopes in soil carbonates, in: Swart, P.K., Lohmann, K.C., McKenzie, J., Savin, S. (Eds.), Climate Change in Continental Isotopic Records. Washington (DC). Geophysical Monograph Series 78, American Geophysical Union, 217–231.

Cerling, T.E., Solomon, D.K., Quade, J., Bowman, J.R., 1991, On the isotopic composition of carbon in soil carbon dioxide. Geochimica et Cosmochimica. Acta 55, 3403–3405.

Feng, J., and Hsieh, Y.P., 1998. Wetlands and aquatic processes; sulfate reduction in freshwater wetland soils and the effects of sulfate and substrate loading. Journal of Environmental Quality 27, 968-972.

Feng, W., Yapp, C.J., 2009. Paleoenvironmental implications of concentration and $^{13}C/^{12}C$ ratios of $Fe(CO_3)OH$ in goethite from a mid-latitude Cenomanian laterite in southwestern Minnesota. Geochimica et Cosmochimica. Acta 73, 2559–2580.

Gastaldo, R.A., Neveling, J., Clark, C.K., Newbury, S.S., 2009. The terrestrial Permian-Triassic boundary event bed is a non-event. Geology 37, 199–202.

Gastaldo, R.A., Knight, C., Neveling, J., Tabor, N., 2014. Late Permian Paleosols from Wapadsberg Pass, South Africa: Implications for Changhsingian Climate. Geo. Soc. Am. Bull. 126, 665–679.

Gluyas, J.G., 1984. Early carbonate diagenesis within Phanerozoic shales and sandstones of the NW European shelf. Clay Mineraology 19, 309–321.

Hsieh, J.C.C., Yapp, C.J., 1999. Stable carbon isotope budget of CO_2 in a wet, modern soil as inferred from $Fe(CO_3)OH$ in pedogenic goethite: Possible role of calcite dissolution. Geochimica et Cosmochimica Acta 63, 767–783.

Montañez, I.P., Tabor, N.J.,Niemeier, D., DiMichele,W.A., Frank, T.D., Fielding, C.R., Isbell, J.L., 2007. CO_2-forced climate and vegetation instability during Late Paleozoic deglaciation. Science 315, 87–91.

Myers, T.S., Tabor, N.J., Jacobs, L.L., Mateus, O., 2012, Estimating soil pCO_2 using paleosol carbonates: implications for the relationship between primary productivity and faunal richness in ancient terrestrial ecosystems. Paleobiology 38, 585–604.

Quade, J., Cerling, T.E., Bowman, J.R., 1989, Development of Asian monsoon revealed by marked ecological shift during the latest Miocene in northern Pakistan: Nature 342, 162–66.

Retallack, G.J., 2002. Carbon dioxide and climate over the past 300 million years, in: Understanding climate change: proxies, chronology and ocean-atmosphere interactions, Gröcke, D.R., Kucera, M. (Eds.), Philosophical Transactions of the Royal Society of London 360, 659–674.

Retallack, G.J., Smith, R.M.H., Ward, P.D., 2003, Vertebrate extinction across the Permian-Triassic boundary in the Karoo Basin of South Africa. Geological Society of America Bulletin 115, 1133–1152.

Romanek, C.S., Grossman, E.L., Morse, J.W., 1992, Carbon isotopic fractionation in synthetic aragonite and calcite: effects of temperature and precipitation rate. Geochimica et Cosmochimica. Acta 56, 419–430.

Royer, D.L., Berner, R.A., Montañez, I.P., Tabor, N.J., Beerling, D.J., 2004. CO_2 as a primary driver of Phanerozoic climate change. GSA Today 14, 4–10.

Sheldon, N.D., Tabor, N.J., 2009. Quantitative Paleoenvironmental and Paleoclimatic Reconstruction using paleosols. Earth Scient Reviews 95, 1–52.

Tabor, N.J., Yapp, C.J., 2005. Incremental vacuum dehydration-decarbonation experiments on a natural gibbsite (-$Al(OH)_3$): CO_2 abundance and ^{13}C values. Geochimica et Cosmochimica. Acta 69, 519–527.

Tabor, N.J., Yapp, C.J., Montañez, I.P., 2004. Goethite, Calcite, and Organic Matter from Permian and Triassic Soils: Carbon Isotopes and CO_2 Concentrations. Geochimica et Cosmochimica. Acta 68, 1503–1517.

Tabor, N.J., Montanez, I.P., Steiner, M., Schwindt, D., 2007. The ^{13}C values of Permo-Triassic carbonates from South Africa reflect a stinking, sulfurous swamp, not atmospheric conditions. Palaeogeography, Palaeoclimatology, Palaeoecology 252, 370–381.

Tabor, N.J., Myers, T.S., Gulbranson, E., Rasmussen, C., Sheldon, N.D., 2013. Light stable isotope composition of modern calcareous soil profiles in California: Implications for CO_2 reconstructions from calcareous paleosols. SEPM Special Publication 104, 17–34.

Thomas, S.G., Tabor, N.J., Yang, W., 2010, Morphology, mineralogy and elemental chemistry of paleosols across the Permo-Triassic boundary in strata from the Turpan basin, Bodga Shan, NW China: revised and accepted by Palaeogeography, Palaeoclimatology, Palaeoecology 308, 41-64.

Yang, W., Liu, Y., Feng, Q., Lin, J., Zhou, D., Wang, D., 2007. Sedimentary evidence of Early–Late Permian mid-latitude continental climate variability, southern Bogda Mountains, NW China. Palaeogeography, Palaeoclimatology, Palaeoecology 252, 239–258.

Yapp, C.J., 2002. Erratum to Crayton J. Yapp (2001), "Mixing of CO_2 in surficial environments as recorded by the concentration and $\delta^{13}C$values of the $Fe(CO_3)OH$ component in goethite," GCA, Vol. 65, 4115–4130. Geochimica et Cosmochimica Acta 66, 1497.

Yapp, C.J., Poths, H., 1991. $^{13}C/^{12}C$ ratios of the Fe(III) carbonate component in natural goethites, in: Taylor Jr, H.P., O'Neil, J.R., Kaplan, I.R. (Eds.), In Stable Isotope Geochemistry: A Tribute to Samuel Epstein, Geochemical Society Special Publication 3, 257–270.

Yapp, C.J., Poths, H., 1992. Ancient atmospheric CO_2 pressures inferred from natural goethites. Nature 355, 342–344.

Yapp, C.J., Poths, H., 1993. The carbon isotope geochemistry of goethite (α-FeOOH) in ironstone of the Upper Ordovician Neda Formation, Wisconsin, USA: Implications for early Paleozoic continental environments. Geochimica et Cosmochimica Acta 57, 2599–2611.

Yapp, C.J., Poths, H., 1996. Carbon isotopes in continental weathering environments and variations in ancient atmospheric CO_2 pressure. Earth and Planetary Science Letters 137, 71–82.

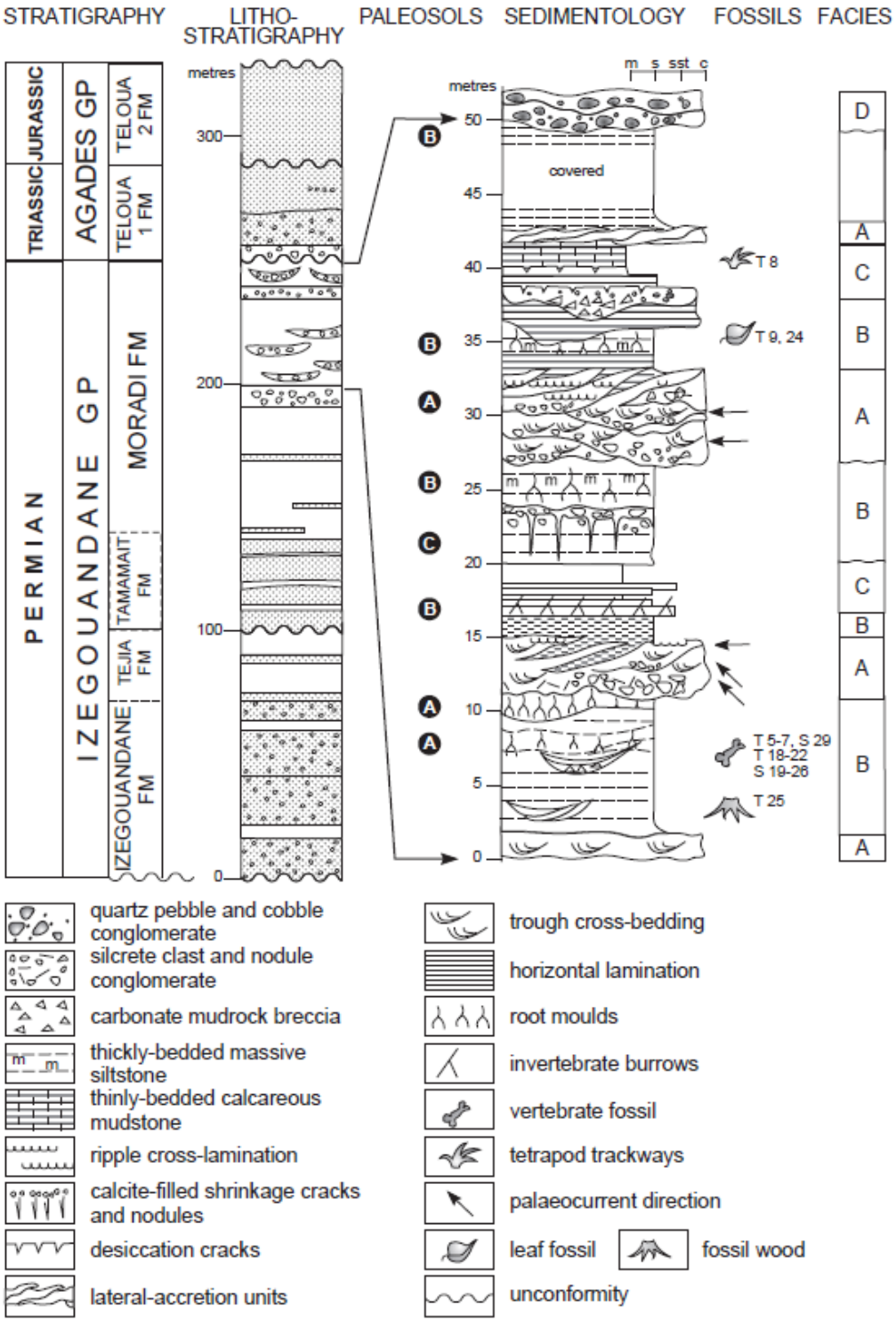

Figure 1

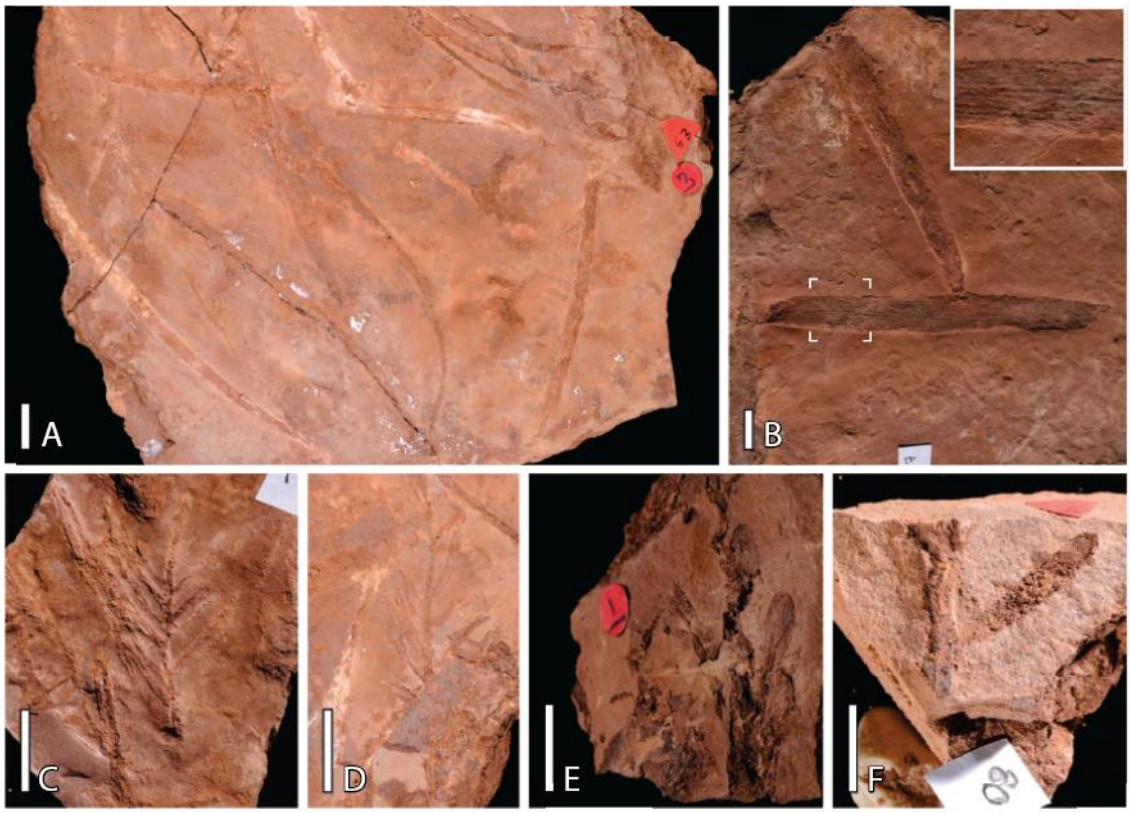

Figure 2

Figure 3

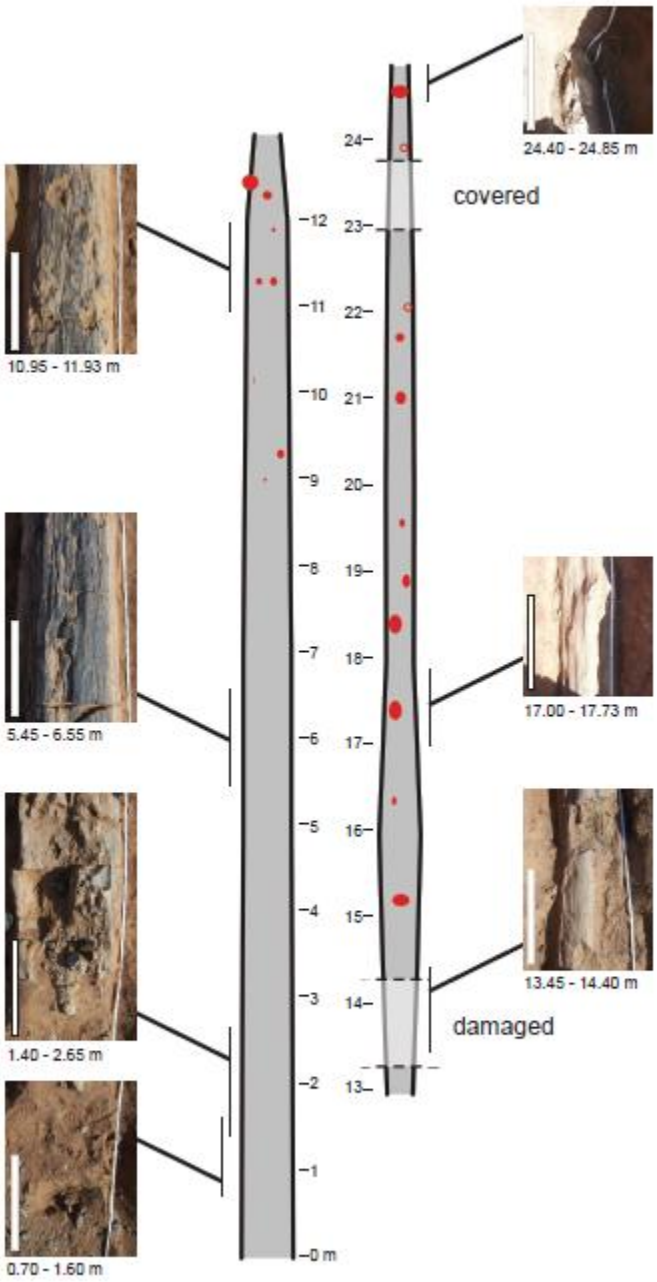

Figure 4

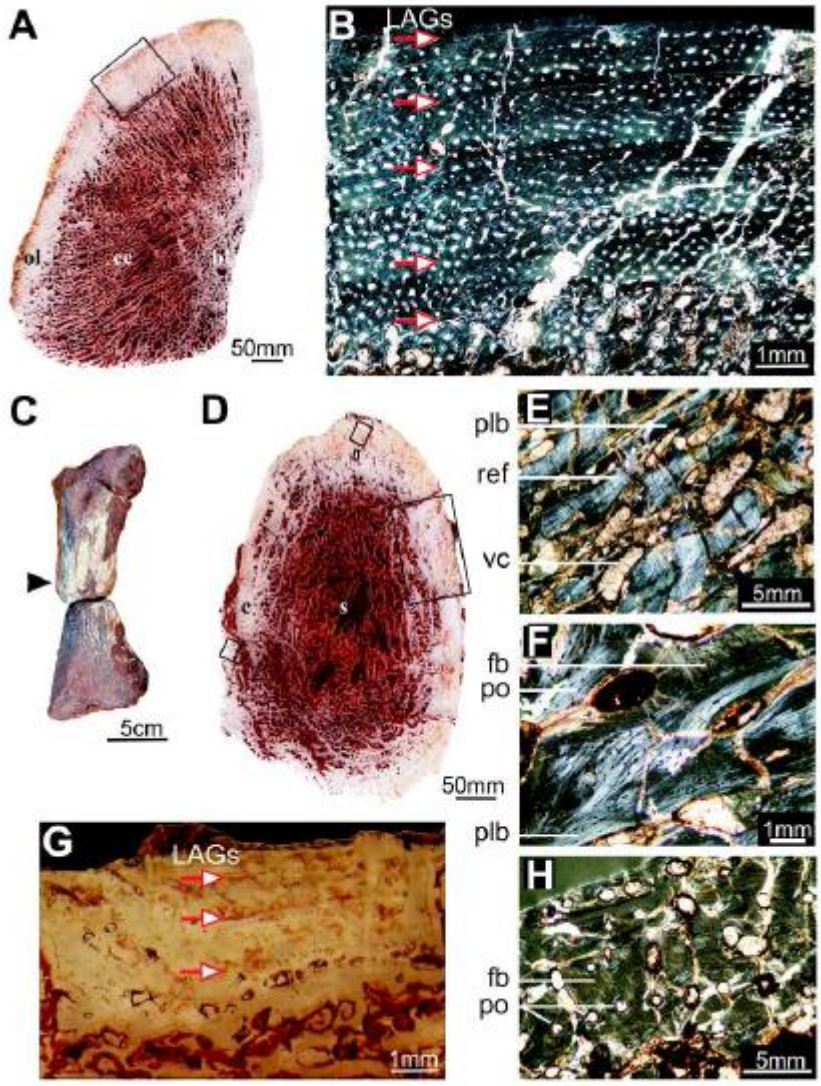

Figure 5

Table 1

Sample	Section	Position in Stratigraphy	Level (m)	Paleosol Type	Host Sediment	Description	Texture	Wt % Calcite	$\delta^{13}C$	$\delta^{18}O$
LMOR1	1	Lower	N/A	A	sandstone	rhizolith	micrite	24.2	-1.9	-6.9
LMOR2	1	Lower	N/A	B	mudstone	Calcans	micrite	52.1	-2.9	-7
LMOR4	1	Upper	N/A	B	mudstone	Calcans	micrite	64.2	-2.9	-7
LMOR8	1	Upper	N/A	B	mudstone	Calcans	micrite	23.2	-3.2	-6.1
UMOR1A	2	Upper	15	B	mudstone	BKII nodules	micrite	78.2	-3.2	-5.8
UMOR1A	2	Upper	15	B	mudstone	BKII nodules	micrite	81.3	-3.3	-5.7
UMOR9A	2	Upper	28	A	mud-ball conglomerate	rhizolith	micrite	88.6	-4.9	-4.3
UMOR9B	2	Upper	28	A	mud-ball conglomerate	rhizolith	micrite	50.2	-5.5	-6.1
UMOR10A	2	Upper	28	A	mud-ball conglomerate	rhizolith	micrite	89.7	-5.5	-5.2
UMOR11A	2	Upper	29	A	sandstone	rhizolith	micrite	93.1	-4	-5.1
UMOR12A	2	Upper	32	A	sandstone	calcrete	micrite	90.6	-3.7	-2.1
UMOR12B	2	Upper	32	A	sandstone	calcrete	micrite	90.9	-4.9	-3.1
2MOR2	3	middle	50	B	mudstone	Calcans	micrite	60.2	-3	-7.9
2MOR6	3	middle	50.5	B	mudstone	Calcans	micrite	56.3	-3.5	-6.4
2MOR6	3	middle	50.5	B	mudstone	Calcans	micrite	56.5	-2.6	-6.3
2MOR8	3	middle	5.2	B	mudstone	BKII nodules	micrite	37.5	-5.8	-8
2MOR9	3	middle	11.7	B	mudstone	BKII nodules	micrite	47.2	-2.6	-7.4
2MOR9A	3	middle	11.7	B	mudstone	BKII nodules	sparite	53.9	-3.4	-7.1
2MOR9B	3	middle	11.7	B	mudstone	BKII nodules	micrite	59.7	-2.6	-7.4
2MOR11	3	middle	27	B	mudstone	BKII nodules	micrite	57.1	-5.2	-3.8
2MOR12	3	middle	40	A	sandstone	Rhizolith	micrite	33.6	-3	-7.9
MOR15A	3	upper	90	A	sandstone	Rhizolith	micrite	100.1	-3.8	-4.2
2MOR15A	3	upper	90	A	sandstone	Rhizolith	micrite	94.5	-3.6	-4.1
2MOR17A	3	upper	98.5	A	sandstone	Rhizolith	micrite	87.5	-3.5	-3.8
2MOR18	3	upper	101	A	mudstone	BKII nodules	micrite	42.7	-1.8	-8.4
2MOR18	3	upper	101	A	mudstone	BKII nodules	micrite	42.7	-1.9	-8.4
MW6	4	middle	N/A	A	sandstone	rhizolith	micrite	89.1	1	1.1
MW6A	4	middle	N/A	A	sandstone	rhizolith	micrite	88.7	-3.8	-4.4

MW7A	4	middle	N/A	A	sandstone	rhizolith	micrite	87.8	-4	-3.6
MW7cc1	4	middle	N/A	A	sandstone	rhizolith	sparite	85.5	-4.6	-6
MW7cc2	4	middle	N/A	A	sandstone	rhizolith	sparite	82.9	-4.6	-6
MW8	4	middle	N/A	A	sandstone	rhizolith	micrite	63.0	-3.3	-4.1
MW8A	4	middle	N/A	A	sandstone	rhizolith	micrite	65.7	-3	-7.2
MW9	4	middle	N/A	A	sandstone	rhizolith	micrite	65.8	-3.2	-4.3
MW9A	4	middle	N/A	A	sandstone	rhizolith	micrite	82.2	-3.4	-3.6
MW9B	4	middle	N/A	A	sandstone	rhizolith	micrite	80.0	-3	-4.2
MW9C	4	middle	N/A	A	sandstone	rhizolith	micrite	51.3	-2.8	-7.1
MW10a	4	middle	N/A	A	sandstone	rhizolith	micrite	99.0	-3.8	-4.2
MW10A	4	middle	N/A	A	sandstone	rhizolith	micrite	99.0	-3.6	-3.7
MW10A	4	middle	N/A	A	sandstone	rhizolith	micrite	99.0	-3.6	-3.8
MW10B	4	middle	N/A	A	sandstone	rhizolith	micrite	89.8	-3.7	-4.8
MW10C	4	middle	N/A	A	sandstone	rhizolith	micrite	85.2	-3.9	-4.8
MW10C	4	middle	N/A	A	sandstone	rhizolith	micrite	63.2	-3.9	-4.4
MW12a	4	middle	32	N/A	sandstone	groundwater concretion	micrite	55.0	-3.7	-4.4
MW13A	4	middle	34.1	A	sandstone	rhizolith	micrite	90.4	-3.4	-3.9
MW15A	4	middle	40.2	A	mudstone	BKII nodules	micrite	100.7	-3.6	-3.6
MW15B	4	middle	40.2	A	mudstone	BKII nodules	micrite	95.2	-3.4	-4
MW15C	4	middle	40.2	A	mudstone	BKII nodules	micrite	94.9	-3.3	-3.7
MW15D	4	middle	40.2	A	mudstone	BKII nodules	micrite	89.8	-2.9	-3.4
MW16A	4	middle	47	A	sandstone	rhizolith	micrite	88.9	-2.4	-4.9
MW17	4	middle	50.6	A	siltstone	rhizolith	micrite	51.9	-2.3	-4.3
MW24	4	middle	64.7	C	mudstone	BKII nodule	micrite	47.3	-1.8	-7.8
MW24	4	middle	64.7	C	Mudstone	BKII nodule	Micrite	19.1	-1.8	-7.8
MW27A	4	upper	75	A	sandstone	rhizolith	micrite	89.4	-4.1	-6.9
MW27A	4	upper	75	A	sandstone	rhizolith	micrite	90.0	-3.6	-4.9
MW27B	4	upper	75	A	sandstone	rhizolith	micrite	47.5	-2.6	-6
MW27	4	upper	75	A	sandstone	rhizolith	micrite	91.2	-3.8	-6
MW28	4	upper	78	A	sandstone	rhizolith	micrite	87.5	-3.7	-6
MW29	4	upper	81	B	mudstone	BKII nodules	micrite	34.2	-2.2	-5.2
MW31	4	upper	84.8	N/A	sandstone	groundwater concretion	micrite	39.5	-0.8	-6
MW32a	4	upper	84.8	A	sandstone	rhizolith	micrite	56.7	-2.5	-4.8

MW32B	4	upper	84.8	A	sandstone	rhizolith	micrite	63.2	-0.5	-0.9
MW33	4	upper	86	B	mudstone	calcans	micrite	31.5	0.5	0.5
MW34	4	upper	94.8	A	sandstone	rhizolith	micrite	67.3	1	2.3
MW35	4	upper	95.5	B	mudstone	BKIII horizon	micrite	75.3	-1.8	-2.3
NW36	4	upper	96.3	B	mudstone	BKII nodules	micrite	71.0	-2.8	-5.3
MW37	4	upper	100.5	B	mudstone	BKIII horizon	micrite	68.5	1.5	3.3
MT7	5	upper	7.5	C	mudstone	BKII nodule	micrite	78.3	-8.2	-10.2
MT8	5	upper	2	C	mudstone	BKII nodule	micrite	55.3	-0.5	-3.7
China – Middle Permian Quanzijie formation										
QF2a	-	-	-	-	mudstone	rhizolith	micrite	82.1	-3.9	-9.4
QF2b	-	-	-	-	mudstone	rhizolith	micrite	71.7	-4.5	-9.9
QF10a	-	-	-	-	mudstone	BKII nodule	micrite	84.3	-5.2	-9.4
QF10b	-	-	-		mudstone	BKII nodule	micrite	77.9	-4.9	-9.9
China – Upper Permian Wutonggou formation										
WY-A1	-				mudstone	BKII nodule	micrite		-10.4	-4.1
TR3-13	-				mudstone	BKII nodule	micrite		-13.5	-8.0
South Africa – Upper Permian Balfour formation										
23606-9a					mudstone	BKII nodule	micrite	35.1	-10.7	-21.5
23606-9b					mudstone	BKII nodule	micrite	35	-9.3	-21.6
21606-8a					mudstone	BKII nodule	micrite	43	-14.4	-14.8
21606-8b					mudstone	BKII nodule	micrite	39	-14.0	-14.3
23606-23a					mudstone	BKII nodule	micrite	46.3	-5.5	-21.3
23606-23b					mudstone	BKII nodule	micrite	47.2	-5.3	-21.0
21606-6a					mudstone	BKII nodule	micrite	42.5	-9.1	-22.2
21606-6b					mudstone	BKII nodule	micrite	50	-15.4	-21.7
21606-1a					mudstone	BKII nodule	micrite	38.7	-15.4	-22.0
21606-1b					mudstone	BKII nodule	micrite	24.7	-17.1	-21.7
Italy – Upper Permian Buntsandstein formation										
JE1a					mudstone	BKII nodule	micrite	*	-4.5	-1.5
JE1b					mudstone	BKII nodule	micrite	*	-4.5	-0.9
JE8a					mudstone	BKII nodule	micrite	*	-5.4	-3.7
JE8b					mudstone	BKII nodule	micrite	*	-5.9	-4.9
JE10					mudstone	BKII nodule	micrite	*	-5.3	-2.8
JE11					mudstone	BKII nodule	micrite	*	-5.0	-2.6

BU3a1	mudstone	BKII nodule	micrite	*	-3.2	-8.9
BU3a2	mudstone	rhizolith	micrite	*	-3.5	-8.9
BU3a3	mudstone	BKII nodule	micrite	*	-3.7	-9.4

*Samples were analyzed by automated common acid-bath on-line system at University of California Davis. This method does not include measurements of wt. % calcite.

Table 2

Sample	Position in Stratigraphy	Paleosol Type	Description	Wt carbon	$\delta^{13}C_{OM}$	$\delta^{13}C_{CC}$[1]	$\Delta^{13}C_{CC-OM}$	Soil PCO_2	AET (mm/yr)
Niger – Middle/Upper Permian Moradi formation									
LMOR1	Lower	A	rhizolith	0.170	-24.3	-1.9	22.4	600	73
MW7	Middle	A	rhizolith	0.329	-23.6	0.8	24.4	500	49
MW18	Middle	A	rhizolith	0.417	-22.7	-3.5	19.2	1000	148
MW19	Middle	A	rhizolith	1.187	-21.9	-2.9	19.0	1100	163
LMOR8	Upper	B	BKII nodule	0.214	-24.7	-3.2	21.5	700	95
UMOR1	Upper	B	rhizolith	0.117	-25.0	-3.3	21.7	700	95
UMOR11	Upper	B	Calcans	0.053	-24.5	-4	20.5	800	114
MW27B	Upper	C	BKII nodule	0.091	-20.8	-2.6	18.2	1300	190
MW37	Upper	B	Calcans	0.098	-24.4	-2.1	22.3	600	73
China – Middle Permian Quanzijie formation									
QF2	-	-	rhizolith	0.620	-19.8	-4.2	15.6	4800	465
QF10	-	-	rhizolith	0.547	-20.3	-5.1	15.2	8000	622
China – Upper Permian Wutonggou formation									
TD83	-	-	BKII nodule		-21.5	-10.4	11.1	N/A	N/A
TR-H2	-	-	BKII nodule		-24.7	-13.5	11.2	N/A	N/A
South Africa – Upper Permian Balfour formation									
23606-9	-	-	Calcans	0.150	-26.1	-10.7	15.4	6000	529
21606-8	-	-	rhizolith	0.097	-25.8	-14.2	11.6	N/A	N/A
23606-23	-	-	rhizolith	0.088	-25.9	-5.4	20.4	800	114
23606-6	-	-	rhizolith	0.071	-26.6	-15.4	11.2	N/A	N/A
21606-1	-	-	rhizolith	0.040	-25.3	-22.0	3.3	N/A	N/A
Italy – Upper Permian Buntsandstein formation									
JE1[2]	-	-	Coaly wood	-[2]	-22.6	-4.5	18.1	1400	203
JE9[3]	-	-	Coaly wood	-[2]	-21.6	-5.3	16.3	2800	335
JE11	-	-	Coaly wood	-[2]	-22.3	-5.0	17.3	1800	248
BU4[4]	-	-	Coaly wood	-[2]	-22.4	-3.7	18.7	1200	177

[1] $\delta^{13}C_{cc}$ values reported in this table are the average of all calcite δ 13C values collected for the sample (see Table 2).
[2] $\delta^{13}C^{OM}$ values for these samples were determined from fossilized organic matter in close stratigraphic association with paleosol calcite samples. These organic matter samples were analyzed with a Carlo-Erba continuous flow Elemental Analyzer interfaced with a Fisons Optima isotope ratio mass spectrometer. This method does not provide an estimate of wt. % organic carbon.
[3] $\delta^{13}C_{cc}$ values are average of JE-1 calcite samples in Table 2.
[4] $\delta^{13}C_{cc}$ values are average of JE-8 calcite samples in Table 2.
[5] $\delta^{13}C_{cc}$ values are average of BU3 calcite samples in Table 2.

Highlights

Biological and physical evidence supports extreme climate in central Permian Pangea
Paleosols and sedimentology indicate aridity with periodic high water availability
Carbon isotopes suggest soil productivity and evapotranspiration were very low
Pareiasaur bones shows evidence of active metabolism and distinct growth marks
The macroflora includes a 25 m long petrified log and voltzian conifer fossils